Mapping Atomic Motions with Electrons: Toward the Quantum Limit to Imaging Chemistry

Zheng Li,[†,‡,#] Sandeep Gyawali,[§,#] Anatoly A. Ischenko,[‖] Stuart Hayes,[‡] and R. J. Dwayne Miller[*,‡,⊥]

[†]State Key Laboratory for Mesoscopic Physics, School of Physics, Peking University, Beijing 100871, China
[‡]Max Planck Institute for the Structure and Dynamics of Matter, CFEL, Luruper Chaussee 149, 22761 Hamburg, Germany
[§]Department of Mathematics and Logistics, Jacobs University Bremen, Campus Ring 1, 28759 Bremen, Germany
[‖]Institute of Fine Chemical Technologies, MIREA - Russian Technological University, Vernadskogo 86, 119571 Moscow, Russia
[⊥]Departments of Chemistry and Physics, University of Toronto, Toronto, Ontario M5S 3H6, Canada

ABSTRACT: Recent advances in ultrafast electron and X-ray diffraction have pushed imaging of structural dynamics into the femtosecond time domain, that is, the fundamental time scale of atomic motion. New physics can be reached beyond the scope of traditional diffraction or reciprocal space imaging. By exploiting the high time resolution, it has been possible to directly observe the collapse of nearly innumerable possible nuclear motions to a few key reaction modes that direct chemistry. It is this reduction in dimensionality in the transition state region that makes chemistry a transferable concept, with the same class of reactions being applicable to synthetic strategies to nearly arbitrary levels of complexity. The ability to image the underlying key reaction modes has been achieved with resolution to relative changes in atomic positions to better than 0.01 Å, that is, comparable to thermal motions. We have effectively reached the fundamental space-time limit with respect to the reaction energetics and imaging the acting forces. In the process of ensemble measured structural changes, we have missed the quantum aspects of chemistry. This perspective reviews the current state of the art in imaging chemistry in action and poses the challenge to access quantum information on the dynamics. There is the possibility with the present ultrabright electron and X-ray sources, at least in principle, to do tomographic reconstruction of quantum states in the form of a Wigner function and density matrix for the vibrational, rotational, and electronic degrees of freedom. Accessing this quantum information constitutes the ultimate demand on the spatial and temporal resolution of reciprocal space imaging of chemistry. Given the much shorter wavelength and corresponding intrinsically higher spatial resolution of current electron sources over X-rays, this Perspective will focus on electrons to provide an overview of the challenge on both the theory and the experimental fronts to extract the quantum aspects of molecular dynamics.

KEYWORDS: *atomically resolved reaction dynamics, key reaction modes, femtosecond time-resolved electron diffraction, time-resolved real-space imaging, quantum tomography, fundamental space time limits to imaging chemistry*
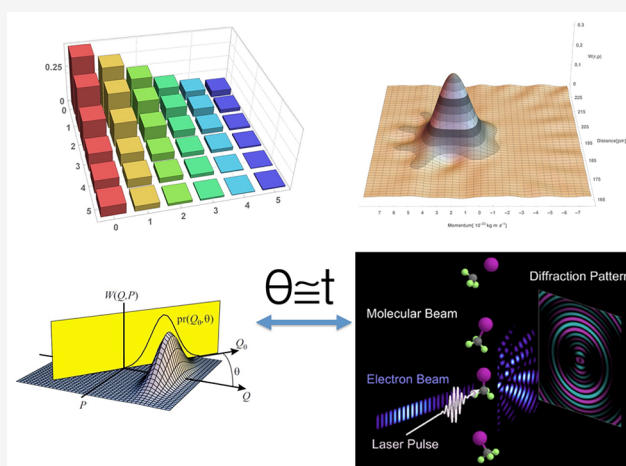
The central unifying concept in chemistry with respect to controlling chemical processes is the notion of a transition state. We try to conceptualize the spatial arrangements of atoms at the critical point defined to be the barrier-crossing region as a means to devise approaches to control the barrier height and thereby gain exponential control over the kinetics leading to the desired chemistry. Trying to picture this special moment in space and time for a given process has provided an important pedagogical tool for guiding chemical strategies for nearly a century, even in the absence of ab initio theory to rigorously describe the process. The idea that we could someday directly observe atomic motions during the defining moments of chemistry would have been thought to be impossible little

more than a decade ago. Given the extremely high spatial and temporal resolution needed to image atomic motions along reaction coordinates, this experiment was thought to be the purest form of a Gedanken experiment. It was even argued by M. Eigen[1] that we could never achieve the necessary imaging technologies to actually see atoms rearrange in space during chemical reactions as he argued that we would always have to use indirect methods for inferring the underlying forces directing

chemistry. This position can well be appreciated by considering the necessary time resolution to catch atomic motions in real time. Consider unimolecular reactions. The prefactor in the Arrhenius expression, which represents the thermal sampling frequency of a barrier between the reactant and product surface (h/kT), is on the order of 10^{13} s^{-1} or 100 fs at room temperature.[2,3] The thermal sampling involves specific reaction modes that direct the transformation from the reactant to the product. These motions are highly damped by anharmonic coupling to the bath during these far from equilibrium excursions sampling the reaction coordinate. The time scale for intramolecular vibrational energy redistribution convolved to this process is also on the order of 100 fs. One can similarly consider the time for two atoms to move along a dissociation coordinate at the speed of sound to within energies of kT of the fully dissociated state to also arrive at 100 fs as the operating time scale.[4,5] This 100 fs time scale is the effective shutter speed needed to observe the reaction modes directing the atomic motions along the reaction coordinate. There are faster chemical processes typically involving strongly repulsive excited state potentials, e.g. photodissociation processes,[6] which do not have time to sample different nuclear degrees of freedom or configuration space. In this case, the time scale approaches the 10 fs time domain with relatively well-defined reaction coordinates. However, for most reactions, the canonical time resolution needed is a few 100 fs to ps time scale. For example, the primary event of vision involves the photoisomerization of retinal in rhodopsin, which is considered to be one of the most evolutionarily optimized, fastest, chemical processes known. This process was initially thought to occur coherently on a 200 fs time scale.[7] It is only recently the reaction has been shown to occur ballistically within 50 fs or a half period of the key torsion mode.[8] The same primary process of photoisomerization of retinal in bacteriorhodopsin occurs within 500−600 fs involving very similar reaction modes but with a less confined excited state potential.[9] Reactions such as electron transfer,[10−12] proton transfer,[13,14] cyclization reactions,[15] and C−H bond activation,[16] basically all reactions in the condensed phase, typically involve medium repolarization or damping of reactive modes by coupling to the surrounding bath on a few 100 fs time scale to ps time scales for the propagation along the reaction coordinate.[17−19] Herein, we will use the 100 fs time domain as the time scale of chemistry.

We note here that there has been some confusion over the separation of the time scales of electronic motions and the coupled nuclear motions. The time scale of changes in electron distribution is on the attosecond time scale. It is this separation in time scale that constitutes the basic physics of the Born−Oppenheimer approximation that allows separating the electronic and nuclear degrees of freedom in treating molecular wave functions. Chemistry is certainly related to changes in electron density. However, the electrons adiabatically follow the nuclear fluctuations not the other way around. If one looks at the partition function for the internal energy of molecules, the energy is predominantly taken up in the nuclear degrees of freedom.[20] The density of states for the nuclear coordinates is higher simply by virtue of their higher mass of the nuclei relative to electrons such that there are many more levels for a given energy range within the nuclear degrees of freedom to store energy. These thermal fluctuations of the nuclei lead to the sampling of the reaction barrier with the electron redistribution adiabatically following the nuclear motion. It is the convolved change in electron distribution to the nuclear fluctuations that

ultimately leads to the dynamic change in the potential energy and forces leading to the resultant chemistry. It is only in the case of processes mediated by a conical intersection[21] or other degeneracies in electronic surfaces, such as weak nonadiabatic couplings typical for electron transfer,[22] where the electronic coupling (giving rise to the change in electron distribution) is small and in which case the electron redistribution for a given nuclear configuration may dominate the time scale for barrier or curve crossing. More correctly, the degree of electronic coupling dictates the transition probability during a nuclear sampled degeneracy between reactant and product surfaces. In all cases, the relevant time scale is still dictated by the nuclear motion to get to that point and then the barrier transmission involves a convolution between the dynamics in the change in electron and nuclear distribution. In this case, the Born−Oppenheimer approximation breaks down and the electronic and nuclear degrees of freedom cannot be separated. The time scale for a given crossing event is still governed by nuclear fluctuations that fall within the 100 fs time domain as opposed to attosecond.

Here we emphasize that the relevant time scale for observing the forces leading to chemistry is on the 100 fs time scale with the above caveat on certain classes of strongly driven photochemical reactions on highly repulsive excited state potential energy surfaces.

Apart from the time resolution requirements, the spatial resolution is equally important. Chemical reactions involve motions on the order of Å's for bond breaking and bond making processes. For chemical reactions involving electron transfer, the barrier is defined by the reorganization energy to stabilize the charge-separated state.[10,23,24] These motions involve normally a large number of intermolecular and intramolecular displacements in response to the reaction field associated with electron transfer,[10,12−14,17−19,24−26] and the magnitude of these motions can be on the order of 0.01 to 0.1 Å.[27−29] This spatial resolution is only nominally within reach with X-ray diffraction methods and is generally more readily accessed with electrons for the simple reason that the de Broglie wavelength of high energy electrons is more than an order of magnitude smaller than hard X-rays typically used for diffraction studies. As a case in point, the most accurate information on bond lengths in molecular systems come from static gas phase electron diffraction studies that can determine bond lengths with a precision of 0.001 Å.[30−33]

The main point is that to image chemistry one needs sub-Å spatial resolution combined with subpicosecond (ps) time resolution. What are the fundamental limits in space-time resolution needed to fully describe chemistry? This limit will be defined by the noise floor that ultimately limits resolving net root-mean-square (rms) atomic motions or more accurately will be defined by the fluctuations on the order of kT that describe the background thermal energy. A chemical process involves transducing stored chemical potential to drive nuclear motions from the reactant surface to the new potential minimum of the product surface. These net motions are larger amplitude than the stochastically driven thermal motions within the reactant surface. We take the fundamental space-time limit to imaging chemistry to be a higher resolution than the rms thermal motions in the spatial coordinate and faster than the effective 1/2 period of the modes that can be used to reconstruct the net motion. Put in another way, this space-time resolution corresponds to fully resolving the reaction forces within kT accuracy. In this respect, the fundamental space-time resolution

to imaging chemistry has been achieved, as will be elaborated below.

We can depict this problem of imaging chemistry as the quest to make molecular movies.[4] Within this analogy, we can more readily relate to the technical challenges to achieve the above space-time resolution. We can discuss the problem in terms of the needed source brightness to achieve the desired space-time resolution or dynamic image contrast. The problem of source brightness was the greatest obstacle to achieving the necessary space-time resolution to imaging chemistry.[31,34] It has been possible for over 100 years now to use X-rays with sufficiently short wavelengths to determine atomic positions and nearly as long a history with electrons to achieve sub - Å resolution. We have also had 100 fs laser systems for over 20 years capable of generating either 100 fs X-ray pulses via plasma generation or similar electron pulses via photoemission for electrons. These sources were all low brightness sources in which only a few X-ray photons or electrons could be detected per pulse using stroboscopic pump−probe methods to stitch together femto-second movies. The very act of a structure change and the need to excite a significant fraction of the sample necessarily makes the sampling process irreversible or there are other limits imposed on the sampling frequency by the time needed for the system to thermally relax back to ambient conditions to avoid accumulated heating artifacts. It was not possible to attain subps dynamics to atomic motions prior to the development of ultrabright electron sources and, 12 years later, ultrabright X-ray sources with the arrival of X-ray Free Electron Lasers (XFELs)[35] for any problem other than fully reversible processes such as exciting phonons in solid state systems.[36−39] These motions are small and the frequencies and curvature of the potential well were known so there was little new information that could be extracted. The goal is to observe motions at far from equilibrium points that lead to transformation of matter from one form to another. Within the typical limitations of finite samples (molecular movie film) and the required number of detected photons or electrons to get above noise, one simply runs out of sample or time to make the measurement.[31,34] The imaging of chemistry really reduced to source brightness. This point can be readily appreciated by considering the lighting requirements for high speed cameras. For a given camera detector efficiency, as one goes to faster and faster shutter speeds, there will invariably be a loss in spatial contrast as the number of photons for capturing the image diminishes to the noise limit needed to fully resolve the object of interest. The image would reduce to ghosts and finally be unresolvable above noise as the shutter speed becomes shorter and shorter to freeze out faster and faster motions. One needs to use brighter and brighter (flashes) to have a sufficient number of photons or electrons in our case to resolve the image. Ultimately one would like to use the brightest, most stable, lighting source possible to image the fastest atomic motions.

At this point, we need to properly define the spatial resolving power with respect to imaging atomic motions. There are a number of different conventions and underlying assumptions in the stated spatial resolution. For real-space imaging, the maximum spatial resolution is simply the Rayleigh criterion for resolving two spatially separated objects, which is just $\lambda/2NA$, where λ is the central carrier wavelength of the source and NA is the numerical aperture of the lens used.[40] In the present context, this relation will only apply to electron microscopy, which is capable of atomic resolution. The de Broglie wavelength is typically less than 0.034 Å for >100 kV electrons.

In practice, the theoretical limit is never achieved due to various limitations in sample, such as electron-induced damage and lens aberrations.[41] There are even greater constraints on the time resolution achievable with real-space imaging with electrons due to time-dependent electron−electron repulsion or space charge aberrations, as will be discussed below. In the case of X-rays, the physical limitations to lens design put atomic resolution out of reach for real-space imaging.

For technical reasons related to information content, the highest spatial-temporal resolution is achieved with diffraction or reciprocal space imaging (vide infra). There are different definitions and conventions used to define the spatial resolution with respect to diffraction observables, which can make comparisons troublesome. In all cases, the resolution is usually interpreted in terms of the largest scattering vector observed. One might assume that simply taking the inverse of this would provide a measure of the resolution, but care must be taken with regard to the conventions used. For gas phase and amorphous materials, the scattering vector is conventionally defined as q (or s) = $4\pi \sin(\theta/2)/\lambda$, where θ is the scattering angle, and the resolution is given by π/q_{max}, which is close to the diffraction limit definition given above in terms of a numerical aperture. This is related to the resolution of a real-space density map that can be formed by Fourier transforming the structure factors, or as more often performed for aperiodic systems, scattering intensities to yield atom-pair correlation functions. In crystallography, it is normal to think in terms of the reciprocal lattice where the magnitude of the lattice- or d-spacing is related to the scattering vector by $q = 2\pi/d$. Data is usually reported in terms of the reciprocal lattice $(1/d)$, and the resolution is defined to be the lattice spacing, d, of the Bragg reflection furthest from the origin within a certain signal-to-noise ratio. This is a measure of the minimum spacing of lattice planes that can be observed and differs from the definition used in gas phase scattering experiments (and the diffraction limit) by a factor of 2. In terms of quantum tomography, the objective is to determine the full nuclear probability distribution. In this case, the specific details of the scattered signal go beyond the definition of resolving atomic positions or centroids in space toward a detailed picture of the shape of the distribution itself, in which case, the resolution limit as defined for aperiodic systems is the relevant definition. From a purely imaging perspective, it is clear, that based on the more than order of magnitude shorter wavelength for current ultrafast electron sources (e.g., 0.034 Å, at 100 keV) over X-rays (~1.5 Å), electrons have the greatest prospect for accessing quantum information on chemical dynamics.

The above defines the inherent spatial resolution. Of course, if there is additional information on the object to be imaged, more details can be extracted from the scattering in either real space or reciprocal space. The other definition of resolution is related to the accuracy of measuring certain structural parameters. By fitting data to structural models within acceptable limits, much smaller uncertainties on the atom positions can be achieved. One is exploiting additional knowledge of the system as opposed to ab initio reconstruction of the image. These approaches rely on some assumptions about the electron probability distribution about each atom giving rise to the scattering. Using this approach within conventional guidelines, the spatial resolution to bond lengths and associated angles in the 3D reconstruction are considered to be much more accurately known than the diffraction limit to resolving uncorrelated objects in space. Convergence to the proposed model or theoretical refinement
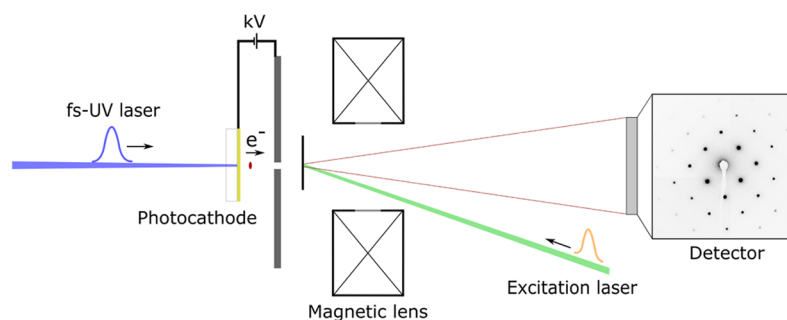
Figure 1. Basic experimental set up of ultrafast electron diffraction.

can give spatial relationships more than one order more accurate than the diffraction limit by exploiting additional information. In this Perspective, we are referring specifically to resolving time dependent changes in atomic structure with known initial structures within this context. The differential change in scattered signal is very sensitive to small changes in atomic position due to the inherent reduced noise through background subtraction. This point needs to be born in mind in the discussion of the resolved structural changes to be discussed below.

In the case of quantum tomographic imaging of chemistry, the objective is to directly determine the wave function probability distribution and its time-dependent evolution during chemical processes, as well as the Wigner function and the density matrix of the quantum wave packet. There is no prior known functional form or information to aid in the image reconstruction. There will be quantum interference effects that are necessarily a many body effect and not simple atomic pair correlations. Important details on the probability distribution will occur on length scales less than atomic bond lengths. Thus, quantum tomography requires ab initio image reconstruction and will push the boundaries to the transform limit to spatial resolution that depends explicitly on a wavelength as defined above. For this reason, the main emphasis of this Perspective is on electron sources. However, we will also point out major advances using X-ray diffraction and novel methods based on internal electron scattering under high field conditions for imaging (vide infra).

MAKING MOLECULAR MOVIES: RECIPROCAL SPACE VERSUS REAL-SPACE IMAGING

The highest spatial resolution, with respect to resolving atomic motions faster than collisions can blur out the acting chemical forces, is obtained using diffraction or reciprocal space imaging. In fact, atomically resolved reaction dynamics have only been achieved with diffraction methods. It is not a matter of technical details to be overcome for real-space imaging but rather differences in the required source intensity for imaging and fundamental limits to intensity prior to the onset of electron induced damage or radiation damage of the sample under illumination.

In the case of real-space imaging, the imaging process is simpler to understand, based on everyday experience using a lens as in a conventional camera to capture motions. It needs to be appreciated that real space and reciprocal space methods are intimately related through their Fourier Transform (FT) relationship. In the case of real-space imaging, as can be readily shown, the lens performs the act of a FT on the scattered source in the lens plane to reconstruct the image at the viewing or recording plane.[42,43] It is only in the case of aberration free

lenses, this reconstruction and image resolution occurs at the diffraction limit of the light or electron source. In the case of diffraction, it is the diffraction pattern that is recorded and subjected to a FT from reciprocal space to real space to reconstruct the image in real space. The difficulty in accurately obtaining real space information is the well-known inversion problem which is related to the fact the measurement of the diffraction pattern measures intensity, which depends quadratically on both the amplitude and the phase of the signal field.[44] There is not enough information from just the diffraction pattern to uniquely determine the phase and invert from reciprocal space to real space. Additional information has to be used and be subjected to various tests to determine the level of accuracy. This problem has been extensively addressed in the electron and X-ray diffraction communities. Most of the atomic structures we have for molecules come from diffraction experiments. The method by which the phases are assigned involves either the use of a heavy atom to provide a well-defined reference in which case the diffraction can be uniquely determined or to use molecular replacement models or theoretical refinement to invert the data, such as multi-wavelength anomalous diffraction.[45−48] As briefly mentioned above, this process is subject to various tests between the model/ theory in which the whole diffraction pattern is subjected to a goodness of fit with accepted minimum values for the correlation function in which to determine the accuracy of the resultant structure. This process has been highly automated in diffraction analysis and is the accepted practice. For time-resolved structural dynamics, it is possible to use the known ground state structure and conserved structural elements to uniquely assign the phase and invert from reciprocal to real space as will be discussed below. Extremely high resolution to differential changes in structure can be determined in this manner. The structural basis for analyzing diffraction or reciprocal space imaging is well established and is used in conjunction with pump−probe protocols to provide the structural probe to obtain molecular movies with atomic resolution of chemical reaction dynamics (see Figure 1 for the basic experimental setup).

The key difference to realize with respect to space-time resolution in using reciprocal space imaging over real-space imaging is the enormous amplification in signal-to-noise one achieves over real-space imaging by sampling a large number of identically presented molecular systems in a regular array with known symmetry or crystal structure. The diffraction signal-to-noise ratio scales as N^2, where N is the number of molecules in relation to the background scatter and noise in the detection process.[49] This relation simply reflects the quadratic nature of the diffraction process with respect to the signal intensity. For a

given electron or X-ray energy, there is a well-defined scattering cross section for each atom being probed. The volume element in which there is coherent amplification (in-phase constructive interference) is defined by the elastic or coherent scattering length and the transverse coherence of the source (see below). For femtosecond electron diffraction experiments, the transverse coherence is on the order of 3−10 nm, with a longitudinal $1/e$ coherent scattering length of order 30−100 nm, depending on the electron energy. Within this defined volume element and typical packing densities, the increased scattering probability gives a total coherent signal amplification $>10^6$ over real-space imaging of a single molecule or reaction volume at a single point.[49] The difference is even larger for fully coherent XFEL pulses. For space charge limited electron pulses or bunch charge, the difference in scattering probability for time-resolved studies is further amplified by summing this transverse coherent contribution over the beam diameter ($\sim$100 μm) for diffraction studies relative to the less than 1 μm beam diameters needed for atomic resolution using real-space imaging. This difference leads to another $>10^4$ increase in sampling time for real-space imaging relative to diffraction studies to achieve the same number of detected scattered electrons. It is possible in principle to compensate for this dramatic difference in imaging contrast in relation to the background noise by increasing the source intensity for real-space imaging and averaging over more shots. However, there is a fundamental limit to the scattering interaction that leads to either electron or X-ray induced damage to the sample. It is the inelastic scattering processes that lead to significant bond breaking, ionization, and associated changes in structure. These inelastic scattering processes occur in parallel to the coherently elastic scattering processes that give rise to the image for either real space or reciprocal space imaging. It is the inelastic scattering processes and associated threshold for electron or X-ray induced damage that ultimately limit the dose.[50] The much lower dose required for reciprocal space imaging to achieve atomic resolution is the key difference that opens up the femtosecond domain to atomic exploration.

In the case of X-rays, it is difficult to make an aberration free lens. In contrast, it is relatively straightforward to make magnetic lens and correctors for imaging with electrons. For this reason, transmission electron microscopes (TEM) are the primary tool for real-space imaging. It should be noted that it is possible to use extremely short X-ray pulses to capture an image faster than the ensuing ionization processes can lead to structure changes, so-called diffract before destroy principle.[51] In this case, it is possible to exploit the extremely high spatial coherence of XFELs to focus X-ray pulses on the order of 10 fs down to molecular dimensions with sufficient X-rays to coherently scatter from the object to reconstruct the object from coherent speckle. The resolution is still limited effectively by inelastic scattering that ionizes the molecule during viewing (X-ray pulse duration) to give a highly distorted electron distribution in the coherently scattered X-ray process. It has been proposed to explicitly include the near complete X-ray ionization, yielding some partial coherence that may help in image reconstruction.[52] The distortion and effect of high field gradients at the X-ray focus is unknown such that the spatial resolution will likely be limited to the nm scale in this strong perturbation limit to imaging molecular systems (until attosecond pulses are available to outrun even electron motion).

In the case of electrons, apart from issues of electron induced damage, it is not possible to arbitrarily increase the electron source intensity to obtain sufficient brightness for atomic resolution, especially not on the 100 fs time scale. Electrons are Fermions and undergo electron−electron repulsion that lead to uncorrelated spatial relationships and aberrations in the image reconstruction. This problem is exacerbated in the microscope column where there are crossovers between lenses in electron trajectories that dramatically increase electron−electron repulsion or space charge generated aberrations. This effect limits the overall beam current for imaging. There are fundamental space-time relations for real-space imaging with electrons under realistic sampling conditions for which 100 ps to 1 ns time resolution can be achieved for few nm spatial resolution and scales linearly in the space-time relation.[53,54] For 100 fs time resolution, the best spatial resolution with sufficient edge contrast would approach the micron scale. There is the prospect of using single electron pulses in repetitive stroboscopic sampling to build up image contrast.[55] The problem here is that atomic resolution requires approximately 10^8 detected electrons in repetitive sampling. Thermal effects, and more importantly, sample damage from the laser excitation limit the sampling to far fewer shots than required for atomic resolution. Also, the slow buildup of the image from single electrons occurs on top of other noise sources such as detector readout noise, laser noise, and thermal noise factors. The inclusion of noise in the overall analysis of image resolution has been evaluated for point projection imaging that does not need to consider crossover effects. The total number of shots using repetitive sampling to attain atomic resolution in the single-electron limit would involve well over 10^{10} excitation or photon cycles in the single electron limit for imaging (SNR = 100, see Figure 8 of ref 56). This estimate assumes 100% excitation of the molecule of interest, which is not feasible at the needed peak powers for subps time resolution to avoid multiphoton artifacts (vide infra). The time to collect an image and the fact that few samples can take over 10^6 photon cycles at the high excitation conditions needed to get around the unexcited background scatter make this prospect rather intractable. Real-space imaging at atomic resolution on the 100 fs, or even ns time scale, has yet to be achieved with this approach. We emphasize this point here as there has been considerable confusion in how far the space-time resolution limit for real-space imaging with electron microscopes could be pushed with single electron sources.[57]

The real power in real-space imaging with electrons is the observation of highly correlated structural changes over longer time scales that cannot be addressed over the limited transverse coherence of electron sources using reciprocal space imaging. This imaging mode allows the study of nucleation phenomena, highly correlated processes involved in phase transitions, direct observation of acoustic modes in nano- to microscale objects, mesoscale structural changes/movements, and nonlinear growth dynamics.[57,58] These important classes of problems occur on ns to second and longer time scales perfectly suited for real-space imaging with electrons. These physical phenomena are not possible to study using diffraction by the simple virtue of their aperiodic nature of the key structural changes. By going to high bunch charge (rather than single electron or few electron bunch charges) and extending the pulse duration of the electron source, dynamic TEM (DTEM) images can be achieved with atomic resolution in principle on the 100 ns to microsecond time scale.[54] In this respect, it is important to point out that there has been a major revolution in real-space imaging of biological macromolecules using cryoEM. This breakthrough was due to the development of direct electron detectors with greatly reduced read out noise approaching unit detector quantum

efficiency. The faster readout time also made it possible to reduce beam-induced motion blurring to allow image alignment in single-particle imaging. Atomic resolution for a number of important biological systems has been attained at doses limited by electron-induced damage to approximately $10e/\text{Å}^2$ and involve alignment of typically over 10000 to 100000 single particles to achieve sufficient image contrast (order 10^8 electrons for image reconstruction of macromolecules) above noise to achieve atomic resolution, which is taken to be 2 Å.[59] It needs to be stressed that these images are under cryo conditions such that they are frozen static structures. One is left inferring the structure−function relationship from static structures, a problem that inherently involves dynamics. The use of DTEM at the maximum peak current to avoid space-charge aberrations should be able to directly observe biological functions at the atomic level of resolution on microsecond time scales and longer, the time scale of biology. This approach will require the development of nanofluidics to observe biological processes under physiological conditions. The spatial resolution will depend critically on the window thickness and achievable liquid path lengths to minimize background scatter that otherwise obscures the object of interest.[60−63] This objective is tantalizing within reach. It may soon be possible to observe at the atomic level individual molecular trajectories on the microsecond to ms time scale to such events as DNA unwinding to the capturing of full enzymatic cycles at atomic resolution under biologically relevant times scales and real-life conditions. These are just two representative examples of the potential impact of such a development in connecting the chemistry that drives biological functions.

■ SPACE CHARGE LIMITS TO ELECTRON SOURCE BRIGHTNESS FOR ATOMICALLY RESOLVING CHEMISTRY IN ACTION

To achieve the desired 100 fs time domain for imaging chemistry, the brightness condition is imposed on the generation of electron pulses with subpicosecond duration. These pulses need to be focused down to 100 μm beam diameters for diffraction to serve as the structural probe for typical excitation beam parameters, which places a condition on finite sample size. Given that most chemical processes are not fully reversible, the number of electrons per pulse or charge density ideally should be sufficient for single shot structure determination. As discussed above, electrons are Fermions and experience intrinsic electron−electron repulsion that will tend to blow up the spatial dimensions of the pulse both in the transverse and longitudinal directions. This phenomenon is referred to as the space-charge problem and it is the basic physics that limits electron source brightness. In this respect, one needs to also consider the source coherence for imaging.[31] As mentioned above, there is the transverse and longitudinal coherence of the source. The transverse coherence is related to the transverse momentum spread of the electrons, normally determined by the initial photoemission process used to generate the electrons.[64,65] It is related to how far energetically above the work function the photoemission process is and trade-offs in quantum yield for electron generation. The transverse coherence determines the spatial resolution.[64−66] You can think of it as beam divergence in optics. For diffraction, the more parallel the beam (less divergent), the higher the spatial resolution with respect to relating the diffraction pattern to the Fourier components of the object being imaged. Similar considerations apply to electrons. The longitudinal coherence

gives the temporal resolution and is related to longitudinal energy spread in the electron velocity over the mean electron energy ($\Delta E/E$).[67] This coherence must be sufficiently long over the sample volume probed to give coherent diffraction for imaging in reciprocal space. In this regard, the scattering cross section of electrons is on the order of 10^5 to 10^6 higher than X-rays for comparable energies. Rather than mm thick samples for optimal diffraction as for X-rays, samples need to be on the order of 100 nm thin for electrons. The energy spread of a few percent due to fluctuations in acceleration voltages, laser noise, and bunch density are well sufficiently small to give coherent diffraction over typical sample thicknesses.

The time resolution is the main issue. In the process of photogeneration of electron pulses, the nascent electron pulse duration at the moment of photoemission replicates the laser pulse duration used for the photoemission step. The ensuing longitudinal momentum spread causes some temporal broadening but it is really the space charge that primarily limits the pulse duration. There is always a trade off in pulse duration and number of electrons for imaging to achieve sufficient image contrast and time resolution.

Due to space charge limitations, it is fair to say that it was thought to be impossible to obtain electron sources with sufficient temporal brightness for the single shot structure determination. This condition is a requirement for any given source technology to serve as a general imaging tool for atomically resolving chemistry. The investment in XFEL beamlines for this purpose makes the point.[35,68,69] It turns out for the 100 μm diameter beam conditions needed for most femtosecond laser experiments, the greatest space charge dilation effect is along the longitudinal, propagation, and direction of the electron pulse, which determines the temporal resolution.[31,70−73] This aspect to the problem can be understood by considering that a 100 fs electron pulse at birth is only 10 μm full width half-maximum (fwhm) in its intensity distribution along the propagation axis, compared to the 100 μm transverse profile. This difference in length scales for space charge broadening allows one to focus on optimizing the temporal resolution for a given required spatial resolution. The key work that determined the ultimate space-time limit to electron sources was based on an effectively exact solution to the coupled equations of motions for some 10000 electrons,[71] which are sufficient for single shot structure determination of a few nm unit cell systems, as verified experimentally.[70] This work showed two regimes where it is possible to maintain 100 fs time domain pulse durations with sufficient bunch charge density for single shot atomic resolution (see Figure 6 in ref 71). There is indeed space charge broadening occurring during electron propagation, but one does not lose space-time correlation in the electron bunch, with it evolving to an extremely linearly chirped pulse. Basically, the electrons at the front feel a strong repulsive force from the trailing electron distribution and are accelerated. Similarly, the electrons at the back are retarded to the same degree. The electrons at the front stay at the front and the electrons at the back stay at the back. The faster electrons move ahead and the combination of quadratic Coulombic repulsion forces and associated velocity dispersion with respect to electron energy leads to a near perfect linear chirp. This finding is extremely important as one can use standard dispersive electron optics such as radio frequency (rf) gradients or reflectrons to compensate the linear chirp to temporally refocus the electron pulse at the sample position down to approximately 100 fs fwhm pulse durations.[74−78] With the rf timing jitter and temperature-

dependent $t = 0$ position, the overall temporal resolution is typically on the order of 200 fs. New timing electronics, which are correct for temperate-dependent drifts in $t = 0$ has solved this problem, making it possible to resolve <100 fs structural dynamics.[79] To date, the highest time resolution achieved is 150−180 fs, which has been sufficient to resolve the key reaction modes or other relevant dynamics of interest.

This calculation also showed that the pulse broadening is primarily the post-extraction field and slow enough to enable samples to be placed directly at the exit plane, the anode, to obtain the desired electron energy for probing the dynamics of interest.[71] In this case, the electron pulses are only nominally broader than with rf pulse compression and higher extraction fields bring the two regimes to parity in terms of time resolution. In the former case, the pulse compression scheme most often used is based on a hybrid DC electron gun to generate the pulse and an rf cavity for the pulse compression.[71,75−78]

The first structural dynamics measurements made using rf pulse compression were for the classic nonthermal melting problem of silicon,[80] where the source brightness was key due to the irreversible nature of the process and use of ultrathin single crystal Si. This source also enabled the first atomically resolved chemical reaction to give a direct observation of bond formation through the process of electrocyclization with conserved stereochemistry,[15] as well as intermolecular electron tranfer[81,82] (vide infra). In addition, there have been a number of important applications demonstrated in the study of strongly correlated electron effects involved in photoinduced phase transitions[83] as well as more recently mapping out the momentum and energy redistribution in the various phonon branches associated with nonequilibrium electron relaxation processes,[84] as representative examples.

The alternative simpler electron source is referred to as the compact electron gun.[70,71,85−88] This concept has the advantage that it does not suffer from rf timing and associated jitter issues and is no more difficult than conventional femtosecond laser pump−probe experiments albeit with an interesting sub-Å probe wavelength for directly observing atomic motions. This source was the first to realize 100 fs time scale resolution to atomic motions[70] and is now widely in use to study the condensed phase to excited state molecular dynamics.[70,85−93]

A new concept has been introduced that should provide the ultimate limit to time resolution and brightness with non-relativistic sources. The source dubbed The Compact RF Electron Gun involves using the chirp in the rf directly for both pulse extraction and compression using flat top or shaped input laser pulses for the electron generation.[94] This concept is virtually identical to the photoinjectors at major X-ray facilities but uses an internal structure to increase the local field to enable the use of compact solid state rf amplifiers as opposed to MW klystrons. This design has an order of magnitude higher extraction field than DC electron guns and correspondingly allows further increases in the electron bunch charge for the desired transverse-longitudinal coherence for imaging. The first prototypes of this source concept will come on line in the coming year.

Finally, there has been remarkable progress in the development of relativistic electron sources in the MeV range for pushing the time resolution to the 10 fs domain,[95−100] but, even more importantly, by virtue of the smaller scattering cross section for relativistic electrons, enabled the use of the thicker samples up to nearly 1 μm thick.[96] The relativistic nature of the electrons eliminates velocity mismatch limits in the time

resolution for the study of gas-phase processes (vide infra) to provide a window on isolated unimolecular reaction dynamics. These sources require major facilities but offer a distinct advantage in making it possible to study gas phase processes with sub-100 fs time resolution. They may also make it possible to routinely study solution phase reaction dynamics as liquid jet technology is now approaching submicron thicknesses that are compatible with MeV electron penetration depths (vide infra). This advantage could be offset by the development of nanofluidics for TEM applications per discussion below that would also open up solution phase reaction dynamics to nonrelativistic sources, which have the advantage of being accessible using dedicated table top electron sources.

The above discussion is to point out that electron sources have achieved source brightness sufficient for single shot atomic resolution of chemical reaction dynamics. There is a simple relationship for adjusting the transverse coherence. By adjusting the ratio of the laser excitation spot size on the photocathode for electron generation and the electron spot size on the sample, it is relatively easy to tune from few nm to 10 nm transverse coherence lengths.[31,75,76,86] For most systems of chemical interest, the needed transverse coherence is on the order of a few nm (solid state, solution phase, gas phase) for relatively small molecule systems (100−1000 atoms per unit cell). In scaling the problem up to probe larger molecular systems up to say proteins, the unit cell for single crystals is on the order of 10 nm, in which case the number of electrons for the same pulse duration must be reduced by an order of magnitude, and more sample averaging is required to accommodate the needed higher number of diffraction orders.

The fact that it is possible to obtain atomic resolution in a single shot with these sources should indicate just how bright these sources are. Effectively, we have achieved the ultimate electron source brightness for imaging atomic motions via diffraction prior to the onset of space charge aberrations in the spatial and temporal domains. We simply cannot go brighter due to the intrinsic space charge limits. The good news is that, at this limit, we have sufficient source brightness to cover the entire domain of chemical interest under either single shot or close to single shot conditions.

■ MOLECULAR MOVIE FILM: SAMPLES, THE NEW FRONTIER

The source brightness problem has been solved. The frontier now is sample preparation. For solid state systems, this problem is well-known to crystallographers. Over the last several decades, a number of sample preparation methods have been developed for electron microscopy (EM) that give the necessary 10−100 nm thick samples. However, these conventional EM sample preparation methods only need samples large enough to image, with few microns in lateral dimension being sufficient. For time-resolved studies of chemical processes, we need sample diameters of at least 100−200 μm and typically require many such crystals to capture enough time points and signal averaging for sufficient spatial resolution. The simple reason is that the very act of exciting the sample changes the sample, either through accumulated heating under vacuum conditions of such thin samples or due to the photoinduced structural change itself. Normally for static imaging it is electron-induced damage that limits resolution. For time-resolved studies under extremely low average electron beam currents, it is the laser excitation that invariably leads to sample damage. To be clear, the electron peak current is very high. However, the extremely short electron

pulses, relatively large beam diameter, and low duty cycle make these e sources more than 4 orders of magnitude lower in average current density than used in conventional TEM studies (e.g., 1 $\mu A/cm^2$ for fs electron diffraction studies relative to >100 mA/cm^2 for typical 1 μm TEM beam parameters). It is really the laser excitation in time-resolved studies that is the main source of damage. One must also be aware of potentially multiphoton artifacts that must be avoided, which is an important point to be discussed further below. It is essential to keep the laser peak power below 100 GW/cm² to avoid multiphoton processes and ill-defined structural changes, especially multiphoton ionization driven structural changes. These multiphoton accessed states are unrelated to the desired excited state surfaces of interest prepared via resonant one-photon processes. Even in the one-photon regime, laser excitation induced damage occurs either at single shot or through accumulated effects, depending on the magnitude of the induced structural change under study. In all cases, laser-induced sample damage occurs at many orders of magnitude fewer shots than electron-induced damage. The sample becomes the limiting factor. It is for this reason that electron source brightness for subpicosecond electron pulses was the single most important problem to solve to enable essentially single-shot capabilities for the direct observation of atomic motions during structural changes. Now the challenge returns to sample preparation. New methods for making large area thin films, single crystals, and rapid nondestructive ion milling for solid state samples are needed. The other challenge is to develop new solid state chemistry systems that allow exploring specific reactions with different structures to test some of the key concepts in chemistry. Currently, chemical synthesis is intuitively guided by concepts such as steric factors and use of electron donating and withdrawing groups to direct chemistry. The diarylethene photochromic systems offer one such platform to explore these concepts in conjunction with selective modifications to the core reactive diarylethene moiety.[101]

Similar comments can be made about solution-phase reaction dynamics. There are some prospects for the development of nanofluidic cells for use with nonrelativistic electrons to enable the study of solution-phase reaction dynamics.[60−62] The problem is the requirement of very thin windows (on the order of 5−20 nm) to enable sufficient electron transmission as a probe without excessive multiple scattering. With flow conditions, this leads to bulging effects that make the liquid path length approach the micron scale, which is too thick. Multiple electron scattering obscures the structural dynamics with such path lengths. It is like trying to look through snow. Here is where relativistic electron sources may have a unique role to play in helping open up solution phase reaction dynamics to atomic inspection. For energies between 2 and 5 MeV, the elastic mean free path of electrons in water or low-density liquids is approximately one micron, which can be realized with recent advances in jet technology.[102,103] The sample delivery is key to opening up solution-phase reaction dynamics and is a challenge we would like to put forward.

For gas-phase studies, the sample is either a molecular beam of diffusive gas source with an effective sample thickness on the order of 100 μm to provide sufficient molecular scattering to observe changes in diffraction. For nonrelativistic electron sources, the time resolution is limited to many ps by the difference in the speed of light (laser excitation) and the electron probe over these dimensions. The use of tilted phase fronts can be used for velocity matching between pump and probe pulses

for specific geometries.[104,105] In the case of the mismatch between electron probe pulses and laser excitation, the laser excitation pulse needs to be brought in off axis to a significant degree with corresponding tilted phase front using diffractive optics to give a velocity matching along the electron propagation direction, which can reduce this effect to 100 fs in principle.[106,107] The use of titled phase fronts has recently been demonstrated for 100 fs time resolution with high energy reflection studies,[108] which have opened up the study of surface dynamics along with low energy electron sources.[109,110] The problem of velocity mismatch has been solved more generally by the recent introduction of relativistic electron sources, which travel essentially at the same velocity as light through this path length. These studies have been able to achieve 150 fs time resolution with <0.3 Å spatial resolution.[111] This resolution was critical to be able to directly observe motion through conical intersections for the prototypical CF_3I system[111] and dissociation of cyclohexadiene,[112] as well as resolve photodissociation channels for CS_2,[113,114] albeit all under multiphoton excitation conditions. These developments are extremely encouraging as we scale to systems of greater complexity.

The major advantage of gas phase studies is that sample delivery is no longer a problem and can be constantly replenished, eliminating the issue of irreversible sample damage. The gas phase electron diffraction community has studied thousands of molecular systems and much of our understanding of molecular structure in regard to bond lengths used in chemistry originated from gas phase electron diffraction (GED) studies (e.g., refs 32 and 33). In the present context, the most important aspect of previous gas phase studies is that they have provided the methodology for introducing molecules of interest into the gas phase, which is now more or less standardized. Many systems can be studied. There is, however, a limitation in regard to relativistic electrons, since these sources require a major installation to get the power class of electron guns to reach relativistic energies. It needs to be pointed out that there are, in fact, clear advantages of nonrelativistic sources over the relativistic counterpart for this class of experiments by going to very high repetition rates (5 kHz demonstrated).[115] There are at least 2 orders of magnitude higher repetition and sampling rates possible that would dramatically increase the signal-to-noise and structural resolution to this class of experiments. To enable fs GED studies more broadly, it is hoped that titled phase front approaches can be more widely adopted along with new means for introducing large molecular systems into the gas phase to enable table-top versions to open up gas-phase studies in general.

It is now all about the samples and sample preparation of condensed phase systems to make suitably thin, 10−100 nm scale thickness, for electron probes. In the gas phase, the challenge is to go beyond few atom molecules to probe larger molecular systems relevant to scaling chemistry and probe different aspects of chemical principles and scaling in complexity. The ideal situation would be to be able to study the same chemical system in the gas phase and in the solution phase to directly determine the effect of the solvent on chemistry—one of the grand challenges of physical chemistry that now seems to be within reach.

■ SPACE-TIME LIMITS TO IMAGING CHEMISTRY: CLASSICAL CASE

To date, enormous strides have been made in pushing the space-time resolution to chemical processes, even within the sample
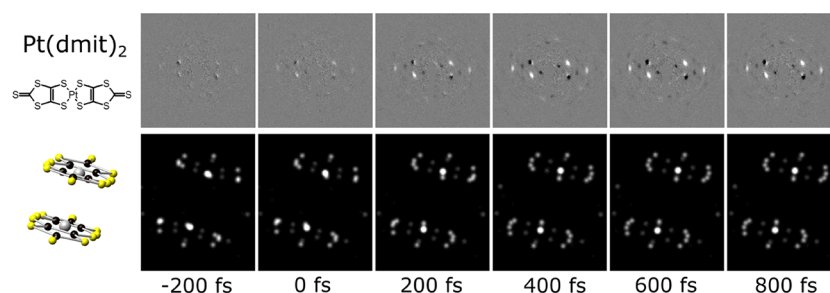
Figure 2. Atomically resolved dynamics of the photoinduced electron transfer in $Me_4P[Pt(dmit)_2]_2$. (Upper panel) Difference electron diffraction data $[I^{laser\_on}(t) - I^{laser\_off}]$ at the specified time delay, t, of the probe electrons with respect to laser excitation. (Lower panel) Real-space dynamics for one molecular dimer derived from the electron diffraction data, in which the relative atomic motions are visible on 100 fs time scales. Adapted with permission from ref 82. Copyright 2015 American Association for the Advancement of Science.

constraints. For this perspective, an atomic movie of structural dynamics is defined to have sufficient space-time resolution to observe net rms motions in atomic positions faster than collisions with the bath (intermolecular or intramolecular) blur out the details.[4,31] The first atomic movie to meet this criterion was the study of strongly driven phase transitions.[116] This work achieved 600 fs time resolution with sub-Å spatial resolution to capture the atomic motions involved in the long predicted phenomenon of homogeneous nucleation. This experiment was the first to exploit high brightness electron sources, using electron pulses with sufficient bunch charge for effectively single shot structure determinations. The number of shots per time point for resolving the atomic motions (changes in radial pair distribution function) was limited by the low quantum efficiency of the detector at the time but it was still possible to see by eye the structural changes on a single shot basis. The basic experimental setup is shown in Figure 1 for the compact electron gun concept. The experimental pump-electron probe protocol is still the same. The only differences are in electron guns (DC-rf, compact electron gun or rf guns), minor changes in electron optics, and perhaps most important use of new electron detectors that are approaching 100% quantum efficiency.

The importance of achieving atomic resolution to structural dynamics was made immediately apparent in the first atomic movie, which focused on atomically resolving strongly driven phase transitions. One could literally watch the transverse motions lead to the collapse of an fcc lattice (Al) to the liquid state in the less than the 1 ps time for full lattice collapse (collective bond breaking between 1.5 and 2.5 ps). The loss of a shear barrier to confine motions defines the liquid state. This difference between solid or glass and the liquid state is taught in physical chemistry in understanding different states of matter. We can now observe this directly. Most importantly, this work discovered the essential physics to strongly drive the phase transitions involved in laser ablation faster than nucleation growth. The new insight into how to arrest nucleation growth provided the long sought solution to the problem of cavitation and shock wave damage in laser surgery, to provide the first tool capable of scar-free surgery at the fundamental (single cell) limit to minimally invasive surgery and with complete biomarkers for surgical guidance.[117,118] These discoveries give testimony to the importance of atomically resolved dynamics not only for its deeper level of understanding of the structural dynamics of matter, but also for the enormous applications that will be forthcoming from such knowledge.

The space-time resolution has improved over the last 16 years to enable resolving coherent motions slaved by electron correlation effects, nonthermally driven phase transitions, to bond formation in electrocyclization reactions, electron transfer in organic and organometallic systems with <200 fs time resolution, and clearly less than the 0.1 Å spatial resolution to the motions.[15,31,34,80−82,90,92,93,111,112,119−121] It has been possible to directly observe the reduction in dimensionality of chemical problems from 100s of possible modes or dimensions to the few key modes that most highly direct the chemical process from the reactant to the product surface.[31,34] As in the above case of simple melting, the atomic level perspective for directly observing the atomic motions directing chemistry has provided a new conceptual basis for thinking about chemistry. The importance of space-time resolution to make this connection needs to be fully appreciated. These modes are the most strongly coupled to the reactant and product electronic surfaces and open the portal between surfaces, that is, direct the barrier crossing. Without sufficient space-time resolution, these motions would not have been resolved. It was the observations of the key reaction modes that pointed out the critical relationship between space-time resolution and the ability to resolve these correlated motions and the enormous reduction in dimensionality that occurs at the critical point of a structural transition. It is this reduction in dimensionality from 100s of potential nuclear degrees of freedom or dimensions to just a few key reaction modes in the transition state region or barrier crossing that ultimately enables chemistry to scale to seemingly arbitrarily complex systems. This point is particularly acute when one takes into consideration the chemistry driving biological functions with greater than 10^4 to 10^5 degrees of freedom for even small protein/enzyme systems. It is the strongly anharmonic coupling between modes, grace of the highly anharmonic nature of the many body potential at crossing points, that leads to localized motions and this apparent reduction in dimensionality.[31,34] It is this relatively simple physics that makes chemistry a transferrable concept that can be scaled to ever and ever larger molecular systems up to the biological scale.

To dramatically illustrate how far the space-time resolution has been pushed with respect to imaging chemical processes, we show in Figure 2 frames of one of the above-discussed molecular movies. The photoinduced electron transfer depicted in this figure is essentially redox chemistry involving electron transfer between organometallic dimers of $Pt(dmit)_2$ (see inset to Figure 2 for the molecular structure). The process of electron transfer is the simplest possible chemistry in that no covalent bonds are made or broken, but in this case it is mediated by changes in

intramolecular bonding and repolarization that stabilizes the charge separated state. There is both inner sphere (intra-molecular) and outer sphere (intermolecular) reorganization involved in the overall medium repolarization.[25] We can now see these motions directly.

This molecular movie was made possible with advances in electron source technology, which in turn highlighted the need for similar attention to be paid to data analysis to provide innovative approaches to extract the most information possible on the reaction dynamics. As in traditional crystallography the well-known phase problem prevents us from directly inverting diffraction data to real space, although the phases can be estimated by assuming they are equal to those in the ground state. In addition, such an approach is restricted by the diffraction limit, but there is a great deal of additional information that can be used to achieve higher resolution. To begin with, it was recognized that we are not trying to solve an unknown structure. We are trying to find the chemical pathway connecting interconverting structures. We know from the observed dynamics that not all nuclear pathways are sampled in the reaction pathway, that is, we know the initial and final structures and what features with respect to bond angles and bond lengths are conserved or are remote from the chemistry of interest. These conserved structural elements are derived from the known structures to serve as experimentally determined constraints. This information is used to build a constrained model using either a few selected modes and fitting this to the data or using a flexible atomistic model with flexible restraints as priors to guide the fitting to the most probable solution (see SI in ref 82). Very few constraints are needed, well within the error bars on the magnitudes of the conserved bond lengths and angles, to lead to unique inversions to real space.

In Figure 2, the atoms are depicted as star like objects against a night sky to not bias your eye, with the brightness scaled according to scattering cross section. Based on the above discussion, the important point to keep in mind is that the atomic motions you can clearly discern in Figure 2 are experimentally derived, not based on MD simulations or ab initio theory, but simply the known electron scattering functions of individual atoms subject to the aforementioned restraints (see also movie link in ref 82, where motion greatly highlights the key modes). In this sense, it can be thought of as a direct reciprocal to real-space inversion with known restraints. As such, this study represents the first full atom resolved chemical reaction. The findings are stunning. One can literally observe directly a 100+ dimensional problem reduce to six reaction modes involving net motions. As anticipated by considerations of the material properties and the fact that the change in electron distribution involves metal centered orbitals, the Pt−Pt distance, and dimer separation are key motions, along with the molecule flatness. Surprisingly, there is an additional tilting of the molecules, which had not been considered beforehand. In all cases, it is the specific motions and equally important that magnitude of the motions that count and can be related to the reorganization energy or driving force for this electron transfer process. The level of detail and clear depiction of the reaction coordinate into its key reaction modes clearly shows the potential of ultrafast electron diffraction (UED) to lead to new insights that might not be uncovered without the aid of a molecular movie to directly observe the time correlated atomic motions.

The specific magnitudes of the motions in the six reaction modes are shown in Figure 3 (see, also, Figure 4). The noise on the signal of the fully relaxed Pt−Pt distance is on the order of
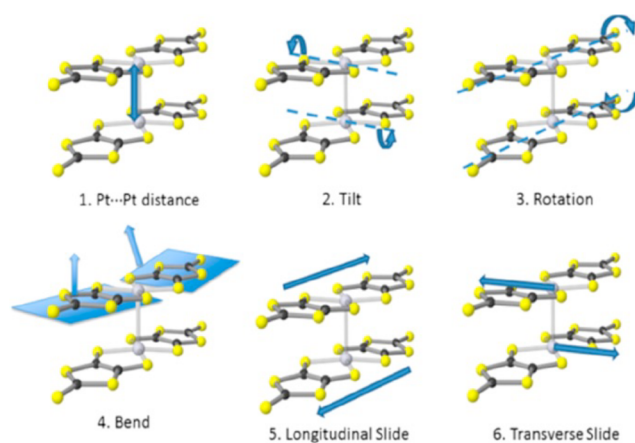

Figure 3. Six dominant types of motion involved in the reorganization process subsequent to photoinduced electron transfer for the organometallic system $Me_4P[Pt(dmit)_2]_2$. Reproduced with permission from ref 82. Copyright 2015 American Association for the Advancement of Science.

about 0.02 Å. The translational motions of the molecules are even smaller at magnitudes of 0.01 Å with precisions on the order of 0.001 Å. The most important point to make with respect to this perspective is that these reaction dynamics were resolved at effectively the fundamental space time to imaging chemistry. The typical reorganization energy is 1 eV. Typically, one has to assume a continuum picture for medium repolarization, or outer sphere reorganization, with the dynamics estimated from longitudinal relaxation times (e.g., solution phase) to think about the outer sphere reorganization and dynamics associated with electron transfer.[10−14,17,24−29] We can now see this directly. Thanks to the single crystal nature of the problem, the specific details are not lost as they would be for a random distribution as in solution phase electron transfer. This is a photoinduced electron transfer process to which there is nuclear reorganization to stabilize the charge separation as in all electron transfer processes. Each of the resolved motions contributes to this reorganization energy. The smallest resolved motions on the order of 0.01 to 0.001 Å are on the same order as thermal motions at room temperature (kT = 25 meV). It is in this sense that the fundamental limit to imaging chemistry has been achieved as we are now at the background thermal noise limit with respect to defining chemically driven atomic motions.

This enormous reduction in dimensionality to a few key modes has been observed in all studies with sufficient sub-ps time resolution to directly observe the atomic motions during the primary events of chemistry. This statement is made in regard to electrocylization reactions involving bond formation with conserved stereochemistry (four dominant reaction modes),[15] intermolecular electron transfer in organic systems (3 or 2 modes),[81,120] and in spin transitions leading to changes in electron distribution that can be modeled as intramolecular reaction coordinates.[121] The aforementioned studies of CF_3I in the gas phase using relativistic electrons is particularly important as it was able to resolve atomic motions thought to be associated with passage through the conical intersection in the one-photon excited state surface leading to dissociation of the C−I bond. Using ab initio theory for refinement, they were able to resolve 0.01 Å motions involving the C−F bond and the excitation of umbrella and vibration modes in the CF_3 product state. The recent fs GED work on the ring opening process for
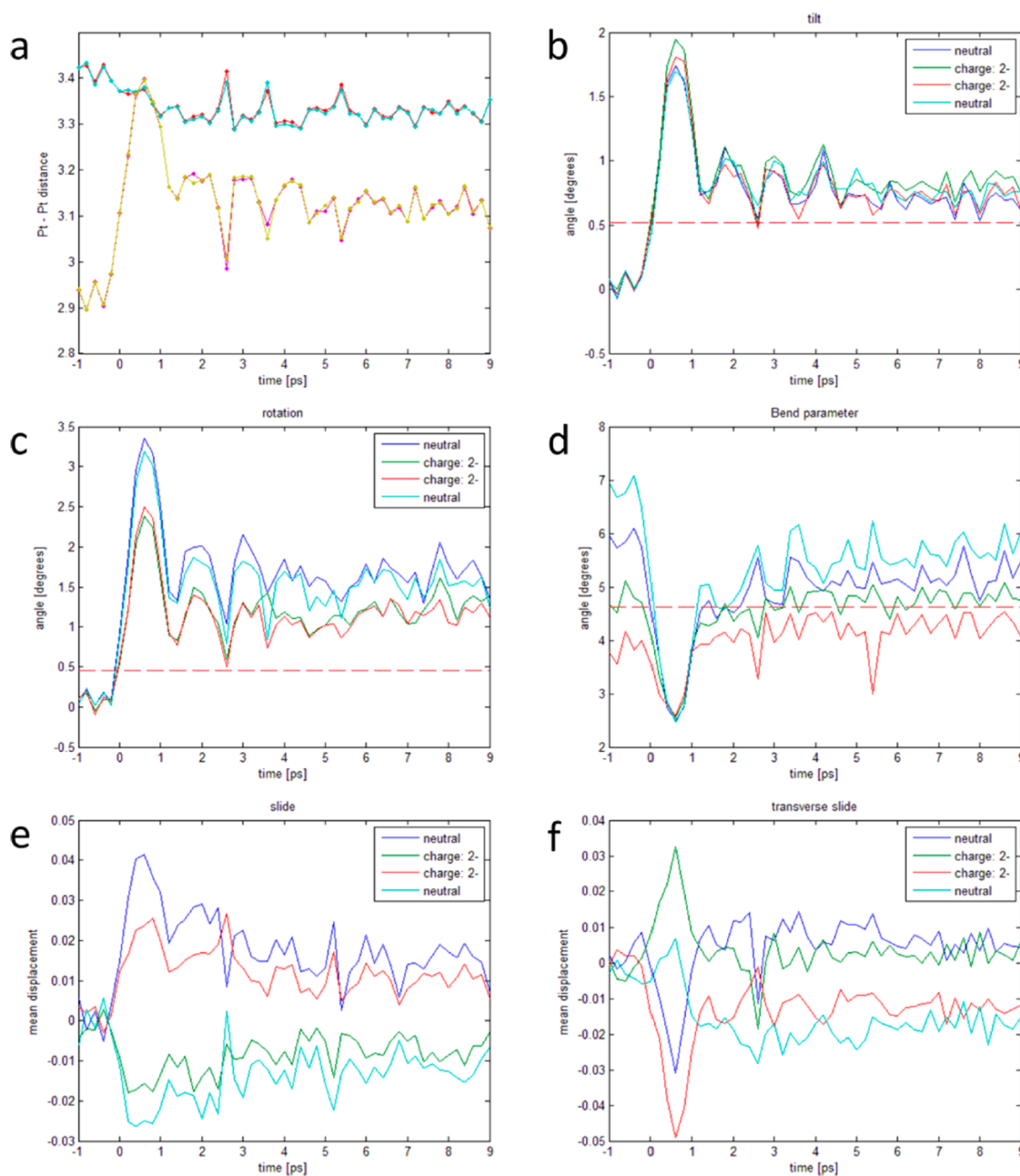
Figure 4. Quantitative analysis of the dominant types of motion coupled to electron transfer between molecular dimers. (a−f) Specific motions 1−6 shown in Figure 3. Adapted with permission from ref 82. Copyright 2015 American Association for the Advancement of Science.

cyclohexadiene was able to follow the dissociation process with 160 fs instrument response function out to s_{max} = 10 Å^{-1} in momentum space to give an absolute image resolution of 0.3 Å. By comparing to ab initio theory they were able to pull out details in the key bond dissociation coordinate. However, this work only reported pair distribution functions. It was not possible to determine specific structural details related to the different stereoisomers that have long been debated for this particular problem (see below). All of the gas phase experiments with relativistic electrons were conducted at excitation conditions well exceeding one-photon transitions, with peak powers sufficient for up to 7 photon processes.[114] The resulting higher excited states will undoubtedly sample different photo-reaction pathways and the branching ratios along different

pathways are needed for proper assignments to specific reaction modes. It will be interesting to compare these findings to conditions involving true one-photon processes to well-defined excited states to separate contributions from high lying electronic states.

The single most important point to take away from the atomically resolved reaction dynamics to date is that there is an enormous reduction in dimensionality in the barrier or transition state region to a few key reaction modes that direct the chemistry.[31,34] It is the relatively simple physics involving strong coupling of vibrational modes at the highly anharmonic components of the potential governing far from equilibrium motions that leads to relatively localized reaction modes. This concept has been used extensively in theoretical treatments of

reaction dynamics to minimize the required sampling of nuclear configurations to make the problems computationally tractable, but properly identifying the key modes is challenging.[122] We can now see these reaction modes directly, and there are always surprises in the details that could not have been anticipated beforehand.

■ COMPLEMENTARY STUDIES

There have been similar developments using different source technologies. The most recent developments with table top X-ray sources and elegant use of passive scattering from the lattice for heterodyne detection have made it possible to achieve 100 fs time resolution to processes involving photoinduced charge motion in the laser field to concerted electron and proton transfer.[123] The spatial resolution to structural changes based on the detected scattering angles and wavelength is on the order of 1 Å; however, using the ground state structure as a starting basis, this approach is sensitive to 0.03 Å changes. The most important aspect of this work was the correlation of the electron−proton transfer steps to changes in electron density that can be retrieved from X-ray scattering. This work was the first to make this connection. There is a limitation in the interpretation of the electron density changes in that it is assumed that these processes occur by a nonresonant two-photon excitation process to the lowest unoccupied electronic state. However, the peak power was in the multi-TW/cm^2 range, where three-photon and higher multiphoton processes may dominate, involving different reaction pathways occurring in parallel. The impressive advances in high power fs IR lasers will increase the X-ray fluence by more than an order of magnitude,[124] and further advances in repetition rate for sampling should enable these studies to be done under one-photon excitation conditions to well-defined excited state potentials to resolve this open issue. The issue of peak power is a common theme for all fs X-ray diffraction studies (vide infra) such that enabling higher signal-to-noise for resonant one-photon excitation alone will be an important development. This is the major challenge right now for femtosecond X-ray diffraction studies.

The largest body of work using femtosecond X-ray diffraction to study reaction dynamics has come in just the past few years from the XFEL community. Interestingly enough, most of this work focuses on the photoinduced chemistry driving biological functions. The methodology is based on serial diffraction in which a large number of different crystal orientations are collected to make up for the fact that the relatively narrow energy bandwidth of XFEL sources leads to incomplete diffraction patterns or partially resolved Bragg peak intensities (partials). These experiments require thousands of crystals to fully resolve reciprocal space for such complex molecular structures to reconstruct to real space for just one time point. A very large number of crystals are needed. In the structural biology community, the conditions for crystallization have been well worked out to enable harvesting the required number of crystals. The first experiments to achieve subpicosecond time resolution to fully resolve the primary processes of the chemistry driving the biological process of interest focused on photoinduced biological processes.[125−130] These works have resolved relatively large amplitude structural changes thought to be involved in the primary processes directing the photoisomerization in Photo-active Yellow Protein (PYP), Green Fluorescent Protein (GFP) conformational changes, the heme doming process involved in ligand dissocation from carboxymyoglobin as part of under-standing oxygen binding and transport of heme proteins, and the

key structural changes involved in the photoisomerization of retinal as part of the primary processes of vision but specifically for the proton transport and energy storage for bacteriorhodop-sin (bR). The structure determination protocol uses a combination of molecular replacement and various levels of theory for structure refinement and for validating the observed structural changes. The diffraction typically goes out in momentum space corresponding to 1.5 to 2 Å resolution. The structural models serve to extend the resolution by taking advantage of effectively known constraints on the protein structure and within this model can pull out changes in structure with resolutions approaching 0.05 Å or less for certain classes of motion. The relative changes in atomic position are model dependent in contrast to the use of experimental constraints as used in the case of Pt(dmit)$_2$ discussed above. Within this limitation, there is wealth of information on cascaded processes that bridge the different time scale of protein motions from the primary event of photoinduced barrier crossing to the structurally encoded deterministic biological function of the protein.

The role of this Perspective is to point out open issues and challenges to the field. In this case, the work is still in its infancy and some caution is needed to properly interpret the observed structural changes in terms of biological relevance. Recent work has shown that, at the excitation conditions and especially peak power conditions, for all of these experiments involve multi-photon absorption to high lying electronic states rather than the assumed one-photon lowest lying excited electronic state.[129] These experiments have used excitation levels corresponding to more than 10 photons/chromophore within the $1/e$ absorption depth and in some cases more than 40 photons/chromophore. The peak powers are all approaching or exceeding 1 TW/cm^2, where additional coherent multiphoton excitation nonresonant processes occur as already noted above and will be greatly amplified under the fully resonant conditions used. These multiphoton excited upper electronic levels undoubtedly sample different reaction pathways and different photoproducts, as is well-known for the bR case (i.e., this effect is specifically used for optical memory[131,132]). The structural changes observed are not biologically relevant as both the reaction pathway and amplitude of the motions will be significantly perturbed by excess energy and driving force for the observed motions. It will be important to redo these experiments under the correct fluence and peak power to ensure true one-photon excitation to the biologically relevant excited states. This condition requires excitation condition of less than 0.2 photons/chromophore within the $1/e$ absorption volume to have less than 10% of the signal arising from two-photon processes. The peak power is an additional consideration even in this limit. For example, saturation of nonresonant two-photon absorption in bR is observed at 700 GW/cm^2 for 800 nm excitation.[131] Under the fully resonant conditions of these experiments (e.g., 530 nm for bR), this multiphoton process will be resonantly enhanced by at least an order of magnitude over the nonresonant case. This class of experiment needs to be conducted at less than 100 GW/cm^2 with peak power studies conducted to ensure the results are biologically and chemically relevant. In order to attain these experimental conditions, the size of the crystals with a given distribution must be on the order of the absorption length, typically less than 10 μm for strongly absorbing transitions (with molar extinction coefficients larger than 10000 M^{-1} cm^{-1}) and chromophore densities. The peak power is still very close to the threshold for nonlinear effects such that crystals on the order of 1

μm may be needed, which is not so different than sample demands for electron diffraction.

The very fact that the noted structural changes were interpreted as biologically relevant with additional theoretical support for the assignments (refs 125, 126, and 128−130) points out how easy it is to misinterpret structural changes that are based on previous time-resolved spectroscopic studies. These comparisons do not examine absolute magnitudes, but rather relative changes in structure to specific regions and dynamics thought to be important. The complexity of the problem leaves open to speculation what motions are most critical to function. New means of assessing the degree of agreement between theory and experimentally resolved structural changes, under well-defined excited state preparation, are needed. As in spectroscopy, to engender confidence in assignments, one needs to consider not only spectral position, but also the amplitudes of all transitions or peaks in the spectrum to avoid focusing only on one or a few spectral features. The full spectrum needs to be analyzed. Similar considerations hold for structural dynamics. The assignment of functionally relevant motions in relation to theoretical predictions must not only consider position, but also amplitude, and the full spectrum of motions to rigorously assign structural changes to biological functions. The degree of theory may not be accurate enough to cast out the full range of key motions, but this can be noted and other probes used to assess functional relevance.

These initial experiments are truly pioneering efforts. The need to refine experimental protocols to improve SNR to go to lower excitation conditions is to be expected. These experiments and advances to theory are key to attaining an atomic level of understanding of the structure−function relationship in biology and finding evolutionary trends in optimally directing chemistry for complex systems on the mesoscale. This issue in separating multiphoton processes from biologically relevant pathways is relatively minor in coming to a final resolution of what makes biology tick.

The most well-defined fs time-resolved experiments of chemical relevance using X-ray diffraction is the work on the ring-opening reaction of cyclohexadiene and a more recent study in fully resolving the structural dynamics of the Rydberg excited *N*-methylmorpholine in the gas phase with sub-100 fs time resolution.[133−136] These studies are particularly impressive examples of exploiting the high flux of XFELs as it was not obvious given the very small scattering cross for X-ray scattering that gas phase diffraction studies would be feasible. This work was able to resolve X-ray scattering out to 4 Å^{-1} and used various levels of theory based on molecular dynamics methods to generate a large number of independent trajectories to which the specific details of the scattered X-ray were compared. The theoretical calculations illustrated that there were significant differences in scattered X-ray q dependence such that it was possible to assign relative weightings to different reaction/relaxation pathways using the theoretically generated basis. It was possible to assign structural changes as small as 0.001 Å (see Table 1 in ref 135, which depends on the level of accuracy of the theory used for essentially structural refinement). This spatial resolution to structural changes is comparable to the previously discussed electron diffraction studies of electron transfer in the Pt(dmit)$_2$ system. The latter case used experimental constraints with measured error bars, which allow absolute accuracy to be judged.[82] In the X-ray diffraction case, it is difficult to determine the level of confidence in the theory used to make these assignments as very small differences in bond length changes

affects the energetics and driving force for the noted structural changes. It will be interesting to test such fits to experimental constraints rather than theory for comparison. In all cases, it is expected that the change in atomic positions should be relatively accurate even if the actual atomic positions, bond lengths, and angles are subject to small corrections. It is the relative change in positions that give insight into the reaction mechanism as is well described in this body of work. The driving force for the reactions will be subject to further refinement with improvements on the theory front. It also should be duly noted that these experiments were conducted at excitation levels on the order of 6% excitation to avoid the aforementioned multiphoton absorption problem. However, given the relatively weak absorptivity, the peak power was still >1 TW/cm^2 to achieve this excitation level and sub-100 fs time resolution. Even though one can rule out uncorrelated multiphoton absorption in the linear excitation regime, there is still the prospect of coherently driven multiphoton absorption at such high peak powers. As with the above XFEL studies, this issue needs to be explored and undoubtedly will soon be resolved.

For completeness, we cite the work on in-liquid X-ray scattering experiments on solution-phase reaction dynamics, which has been extensively reviewed.[137] This class of experiments was the first to illustrate the possibility of attaining atomic resolution of molecular dynamics in solution phase where most chemistry occurs. The challenge is to find a system that has high solubility and scattering cross section to get above the background solution phase scattering that masks the dynamics of interest. To date, studies have included photoinduced bond formation using the aqueous Au-cyanide trimer as a model system[138] to exploit the high scattering cross section of Au. This work resolved changes in the solution phase scattering interpreted as bond contraction and linearization within a few 100 fs, further bond contraction within 2 ps, and Au−Au bond formation to give a tetramer on ns time scales. There is a disagreement with previous assignments based solely on transient absorption studies. To our read there is a bit of controversy here, as both cases rely on theory and accurate ab initio treatment of Au electronic effects is nontrivial. Similarly, there have been studies on metal organic systems involving photoinduced changes in electron distribution and bonding at metal center orbitals for better understanding photocatalysts (e.g., [Ir$_2$(dimen)]$^{2+}$, where the dimer is *para*-diisocyanomenthane), as well as probe solvation dynamics.[139] There have also been studies that have proposed high vibrational excitation through resonant Raman scattering to probe highly excited ground state vibrational wavepacket dynamics for the diplatinum anion (Pt$_2$POP$_4$).[140] There is a common underlying concern for all the in-liquid X-ray scattering studies. The excitation conditions for all these experiments were conducted at far too high excitation conditions for solution phase studies (>1−2 TW/cm^2 in the X-ray probed volume). The high excitation and peak power conditions were presumably used, because it was not possible to observe signal under rigorously single photon absorption levels. For solution-phase conditions, in particular, these excitation parameters have been well characterized by the femtosecond community to follow the guidelines given above to ensure one-photon excitation conditions. There is an additional caveat in that the solution phase background is subject to nonradiative relaxation processes and time dependent changes in solvent temperature and parameters. This time-dependent background scatter is very difficult to properly subtract to obtain the relatively diffuse

photoactive solute parameters (atomic pair distribution functions) of interest. It is not possible to do the necessary controls without the solute and still deposit the same energy on the same time scale to rigorously remove this time-dependent baseline scattering. Various methods have been tried, with most relying on MD or assumed thermal relaxation dynamics and scaling parameters. The problem is that the peak power is high enough to significantly excite upper level, short-lived, excited states of the solvent itself, as well as photoionize the solvent and solute, to give rise to competing solvated electron chemistry. At these peak powers, ionization of the photoactive chromophore or solute needs to be taken into account. It is not clear at present how to rigorously separate these effects and connect the observed changes in X-ray scattering to the reaction dynamics of interest, especially for observables invoking the observation of solvation dynamics. These multiphoton effects may not alter the general conclusions but the details matter with respect to understanding the reaction forces. With the higher repetition XFEL sources coming on line, it should be possible to increase the signal-to-noise to allow true one-photon excitation conditions to better define the solvent contribution and extract the molecular dynamics of interest. The use of X-ray scattering to study solution phase reaction dynamics is clearly a very important area in chemistry and we can expect major progress in this area using both electron sources with newly developed nanofluidics and XFEL sources.

The ultimate time resolution for either X-ray or electron sources has been attained with attosecond laser methods using laser-induced electron diffraction (LIED) to achieve <0.05 Å resolution with sub-fs time resolution to high field electron ionization processes, even resolving proton motions.[141] To date, the photodissociation of diethylene[141] and Renner-Teller distortions of CS_2 have been studied,[142] as well as distortion of isolated water molecules involving bond distortion and breaking under high field conditions.[143] The spatial resolution to the ensuing nuclear dynamics under strong field conditions requires an assumed exit wave function for the scattering electron. As such, the structure determination depends entirely on the assumptions of the scattering wave function. These high field conditions are not chemistry per se but are interesting in their own right for probing light-matter interactions under strong field conditions. There are prospects this approach can be extended to following photochemical processes using the LIED process as a probe at various time delays. It will be extremely interesting to see how this field evolves and if the method can be extended to larger molecular systems of chemical interest.

TOWARD QUANTUM LIMITS

The above discusses our current limits and the direct observation of the enormous reduction in dimensionality that occurs during barrier crossing in chemical processes. It needs to be fully appreciated that the above details were all ensemble measurements in which the observable in the image reconstruction process was the center-of-mass positions of the atoms. The picture of the atomic motions in this sense is strictly classical. The ability to pull out the key modes from the structural changes effectively projects out the motions most strongly coupled to the reaction coordinate. We should add that we know there is a distribution of nuclear motions, most of which are orthogonal to the reaction coordinate or spectator modes. We do not resolve them as net relative motions or displacements. Many of these motions likely average out as each trajectory samples slightly different combinations of motions.

These differences will cancel out in an ensemble measurement, much like thermal noise, in assessing the center of mass positions of the atoms in structure determination. They are therefore unobservable. This cancellation effect in a way helps focus attention on the most important aspects of the reaction coordinate. The ensemble averaging reinforces or rather really lights up the key reaction modes that are common to all the trajectories sampled in the ensemble. In this respect, these ensemble observations help reduce the problem to the most important motions.

However, there is still the desire to push the space-time limit to imaging chemistry even further. We know there are quantum effects that influence the chemistry. What are the quantum limits? The above discussion treats the problem strictly kinematically in which the process, although quantum in nature, is viewed classically as well-defined (ensemble average) changes in atomic position. In an ensemble measurement, the system can converge to well-defined average values. However, underlying these net average motions are the quantum aspects. We would ideally like to access the nuclear probability distribution and reconstruct time dependent wave functions. This information is contained within the diffraction data through the corresponding distribution in scattering of sub-Å sources used for imaging the atomic motions. This information is not currently accessible except for very simple cases, as we do not know how to extract the probability distribution uniquely from the scattering intensity. The basic problem belongs in the realm of quantum tomography and the problem reduces to something very similar to solving the phase problem in conventional diffraction data in transforming to real space. One needs additional information to solve for the phase for a multivariable diffraction problem. Ditto for quantum tomography. How can we access this information and what are the limitations?

QUANTUM TOMOGRAPHY

In this section, we would like to explore the idea of going beyond what is essentially a classical description of the atomic motions involved in chemical processes. There is more information in electron scattering (or X-ray) as it is effectively a quantum scattering event. From a quantum perspective, what is the ultimate information limit we can retrieve about molecular dynamics and chemical processes? We will focus on electron scattering as there are fundamental limits on X-rays for typical energies used to address this issue.

In accordance with the basic principles of quantum mechanics, the state of a single molecule cannot be determined experimentally. However, for an ensemble of identical systems it is possible to determine their density matrix. Knowing the status of the system means that we have the most information about all physically measurable quantities. The density matrix and the probability density function in the corresponding phase space, the Wigner function, have a one-to-one correspondence, which describes the maximum of the available statistical information. Therefore, when the term molecular quantum state is used, the quantum state of the ensemble of molecules is assumed.

In 1933, it was demonstrated that a pure quantum state $|\Psi\rangle$ can be recovered from the time-dependent probability density function $P(r, t) = |\psi(r, t)|^2$ and its derivative $\partial P(r, t)/\partial t$. Pure quantum states can also be recovered by measuring P(r, t) at time t and its time sequence (evolution) through fairly short intervals Δt, that is, as shown in $P(r, t + N\Delta t) = |\psi(r, t + N\Delta t)|^2$, ($N = 0, 1, 2, ...$).[144,145]

Scattering intensities in UED have a direct correlation with the time-dependent probability density function of internuclear distances $P(r, t)$. In UED a pulsed electron source is utilized for probing the ensemble of particles in a certain time sequence. Synchronized electron and laser pulses provide a stroboscopic picture of the evolving process. Thus, an additional variable is introduced into the measurements, which is time. It becomes possible to study the coherent dynamics of the nuclei in the laser-excited systems, the transition state of the chemical reaction, and the dynamics of molecular wave packets. UED can be utilized for probing dynamics of wave packets, coherent superposition of quantum states, created by short optical pulses with controlled phase. Consequently, it becomes possible to directly observe the coherent nuclear dynamics of excited molecules as a single act of the elastic electron scattering occurs on the attosecond time scale.

The time-dependent intensities of molecular scattering of electrons obtained using UED with coherent excitation of the molecular system, provide the possibility of determining the fundamental elements of the density matrix and the tomographic reconstruction of the molecular quantum state of the system.

In classical mechanics, there are no equations describing the evolution of the probability density function $P(r, t)$ and $P(p, t)$; only the joint probability density function, $W_{cl}(p, r, t)$, can be expressed using the Liouville equation. Therefore, there are no corresponding quantum equations for $P(r, t)$ and $P(p, t)$. However, the known Wigner-Liouville equation can be used to describe the evolution of the Wigner function, $W(r, p, t)$.

The UED molecular intensity function, $I_M(\mathbf{s}, t)$ can be written as[146]

$$I_M(\mathbf{s}, t) = \mathbf{Re} \sum_{i \neq j} |f_i| |f_j| \cos(\eta_i - \eta_j) \int d\mathbf{p}_{ij} \int d\mathbf{r}_{ij} W(\mathbf{r}_{ij}, \mathbf{p}_{ij}, t) \exp(i\mathbf{s}\mathbf{r}_{ij}) \quad (1)$$

where f_i and η_i are the amplitude and phase of scattered electrons for atom i. $\mathbf{r}_{ij}$ is the internuclear distance and $\mathbf{s}$ is momentum transfer of the scattered electron. $\mathbf{Re}$ denotes the real part. Further, we will denote $|f_i||f_j|\cos(\eta_i - \eta_j) = g_{ij}(s)$.

Equation 1 is the most general representation of the intensity of the molecular scattering in UED, expressed in terms of the Wigner function, $W(r, p, t)$. In this representation, $I_M(s, t)$ can be interpreted as a filtered projection of the Wigner function, where the scattering operator $\exp(i\mathbf{s}r)$ is a filter, modified by scattering functions $f(s)$. For many problems, the Wigner function can be derived in analytical form (see, for example, ref 147) or by solving the Wigner-Liouville equations numerically with the corresponding potential function of the molecule.

The Wigner function in eq 1 can be expressed as

$$P(r, t) = |\psi(r, t)|^2 = \int dp W(p, r, t) \quad (2)$$

In general, it is assumed that $\psi(r, t)$ can describe a mixed quantum state, where $\mathbf{r}$ are canonical coordinates of the system in the phase space. In the case of electron diffraction, these are interatomic distances, $\mathbf{r}_{ij}$. The wave function $\psi(r, t)$ can be represented as an expansion in orthonormal basis functions $\psi_n(r)$ as follows:

$$\psi(r, t) = \sum_n C_n \psi_n(r) \exp(-i\omega_0 t) \quad (3)$$

where n is the quantum number of states with energy E_n, ω_n is the frequency of oscillations, and C_n is the probability amplitude. Then, eq 1 can be written as

$$I_M(\mathbf{s}, t) = \sum_{i \neq j} g_{ij}(\mathbf{s}) \sum_{mn} \rho_{mn} \exp[i(\omega_m - \omega_n)t] \langle \psi_m(r)|\exp(i\mathbf{s}r_{ij})|\psi_n(r)\rangle \quad (4)$$

where ρ_{mn} is the elements of the density matrix.

Equation 4 shows that the intensity of the molecular scattering explicitly depends on the quantum state of the molecular system. Accordingly, the probability density function $P(r, t)$, which can be obtained using UED data as the Fourier transform:

$$P(r, t) = (2/\pi)^{1/2} \mathrm{Re} \int ds I_M(\mathbf{s}, t)[g(\mathbf{s})]^{-1} \exp(-i\mathbf{s}r) = (2/\pi)^{1/2}$$
$$\times \mathrm{Re} \sum_{mn} \rho_{mn} \exp[i(\omega_m - \omega_n)t] \int ds \langle \psi_m(r)|\exp(i\mathbf{s}r)|\psi_n(r)\rangle \exp(-i\mathbf{s}r) \quad (5)$$

which depends on the internuclear distance $\mathbf{r}$ and time t, and explicitly contains all the information about the quantum state of the system and represents a projection, or "shadow", of the Wigner function.[148]

The interference term in the intensity of molecular scattering of electrons (eq 1 and its Fourier image, eq 5) gives, in principal, the possibility for determining the density matrix $\boldsymbol{\rho}$ and performing a tomographic reconstruction of the molecular quantum state of the system.[149] Therefore, the temporal sequence of measurements of scattering intensity $I_M(s, t)$ and the Fourier transform (eq 5), which transforms from the space of scattering variable s into the space of interatomic distances r, provides the required information for the tomographic reconstruction of the Wigner function $W(r, p)$. For this purpose, the Radon transform may be utilized:[149]

$$W(r, p) = -\frac{P}{2\pi^2 \hbar} \iint dx d\theta \frac{P(x, \theta)}{(r \cos \theta + p \sin \theta - x)^2} \quad (6)$$

where P is the Cauchy principal value and $\theta = \omega t$ is the angle of rotation in the phase space, corresponding to the time of motion t on the potential energy surface of the molecule.

In eq 6, the integration should be performed in the range of $0 \leq Q \leq 2\pi$. This means that, for determining the full quantum state of the system, the measurement should be performed using UED to generate a "tomographic complete" set, in which a full period of reconstruction of the wave packet, T_{rev}, takes place,[150] that is, in the interval, $0 \leq t \leq T_{rev} = 2\pi/\omega$, which corresponds to a complete cycle of rotation of the Wigner function. When using the full data set for tomographic reconstruction of a coherent state the wave packet at $t = 0$, the Wigner function, $W(r, p, 0)$ can be recovered using the inverse Radon transform, eq 6. Similarly, by taking measurements of the scattering intensity in the time interval of $0 + Nt_d \leq t \leq T_{rev} + Nt_d$, where N is an integer and t_d is the delay of the electron pulse from the laser pulse, the Wigner function can be restored for time, Nt_d. Therefore, UED provides the capability for recovering the quantum state of the molecules in the ensemble.

Another method for recovery of the molecular quantum state is determining the elements of the density matrix, ρ_{mn}, which have a one-to-one correspondence with the Wigner function:[151]

$$W(r, p) = (1/\pi\hbar) \int \exp(2ipx/\hbar)\langle r - x|\rho|r + x\rangle dx \quad (7)$$
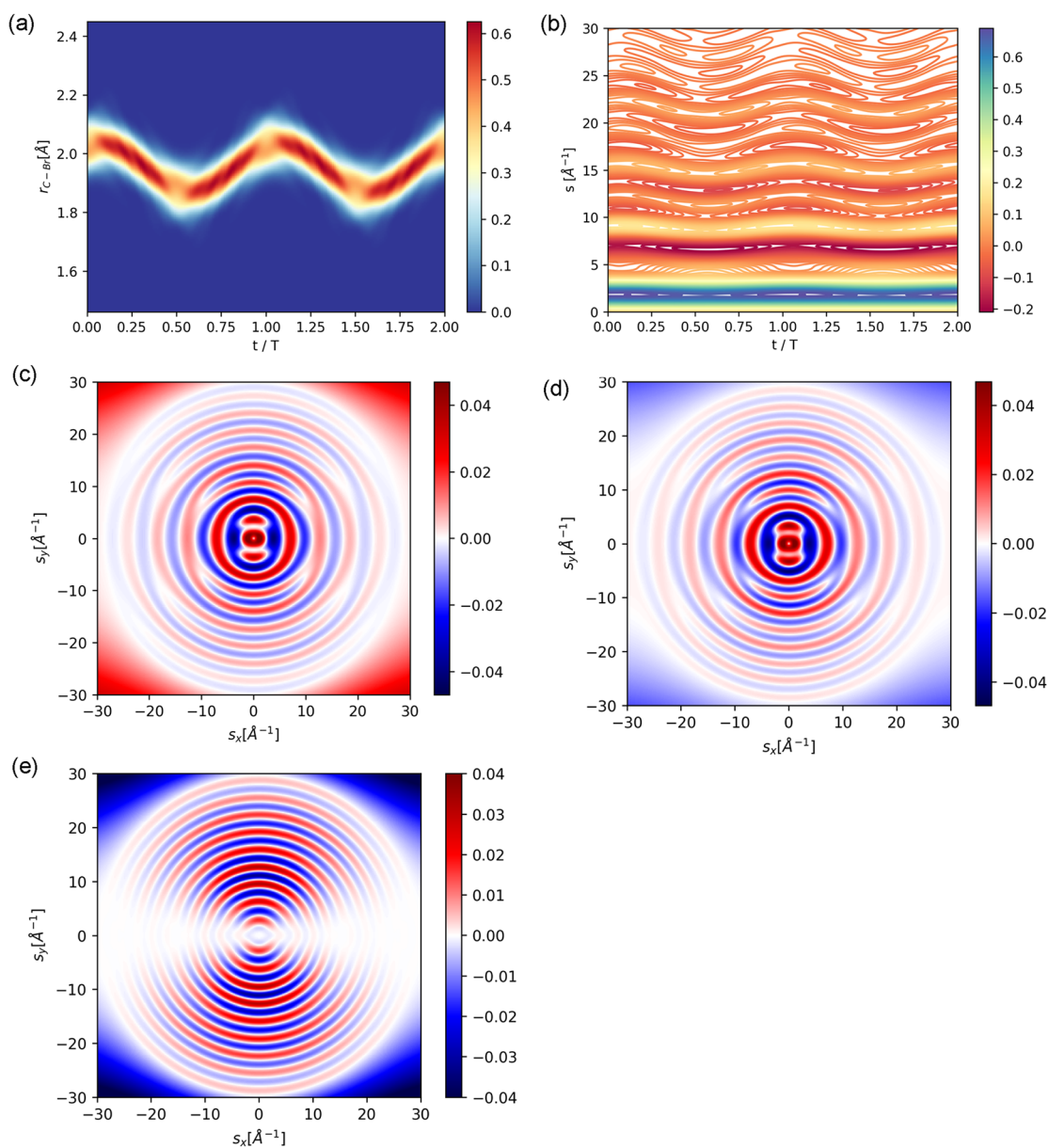
where ρ is the density matrix:

Figure 5. (a) Simulated probability density (scale bar) of a coherent vibrational wavepacket of CH_3Br^+ on the electronic ground state, where T is the oscillation period and r is the C−Br distance in Å. (b) Isotropic molecular scattering intensity $sM(s, t)$ for the wave packet as a function of the magnitude of momentum transfer s for the first two periods. White in this figure was added for contrast to see the dynamics. (c) A simulated electron diffraction pattern, $sM(\mathbf{s})$ at $t = 0$ for the excited fraction of a gas-phase sample of CH_3Br assuming a $\cos^2 \theta$ distribution and a linearly polarized laser pulse parallel to the y-axis of the detector. (d) Simulated electron diffraction pattern, $sM(\mathbf{s})$, for the excited portion of CH_3Br at $t = T/2$. (e) Difference between the molecular scattering intensity at $t = 0$ and $t = T/2$.

$$\rho = \sum_{nm} \rho_{nm} |\psi_n(r)\rangle\langle\psi_m(r)| \qquad (8)$$

In the case when the measurement is performed for an incomplete cycle, as determined by the time interval $0 + Nt_d \leq t \leq T_{rev} + Nt_d$, then only the diagonal elements of the density matrix can be determined. Determination can be performed using a probability density function $\langle P(r, t)\rangle_\tau$, averaged over the time interval $\tau \gg \sup(|\omega_m - \omega_n|^{-1})$, $m \neq n$, as was demonstrated in[148,152]

$$\rho_{nn} = \int dr \langle P(r, t)\rangle_\tau \frac{\partial[\psi_n(r)\varphi_n(r)]}{\partial r} \qquad (9)$$

where $\psi_n(r)$ is a regular normalizable solution of the time-independent Schrödinger equation and $\varphi_n(r)$ is the second linearly independent innormalizable solution.

The prospect of extracting nuclear probability distributions was first discussed in the context of one-dimensional problems involving dissociation,[153] which has recently been demonstrated for I_2.[154] We need to extend the dimensionality of the problem to obtain quantum information for multiatom systems to truly address chemical processes. Ideally, we would like to directly observe the quantum aspects of the intrinsic reduction in dimensionality within the quantum system that leads to a few key reaction modes directing chemical processes. This must have quantum origins. To better pose the problem in this
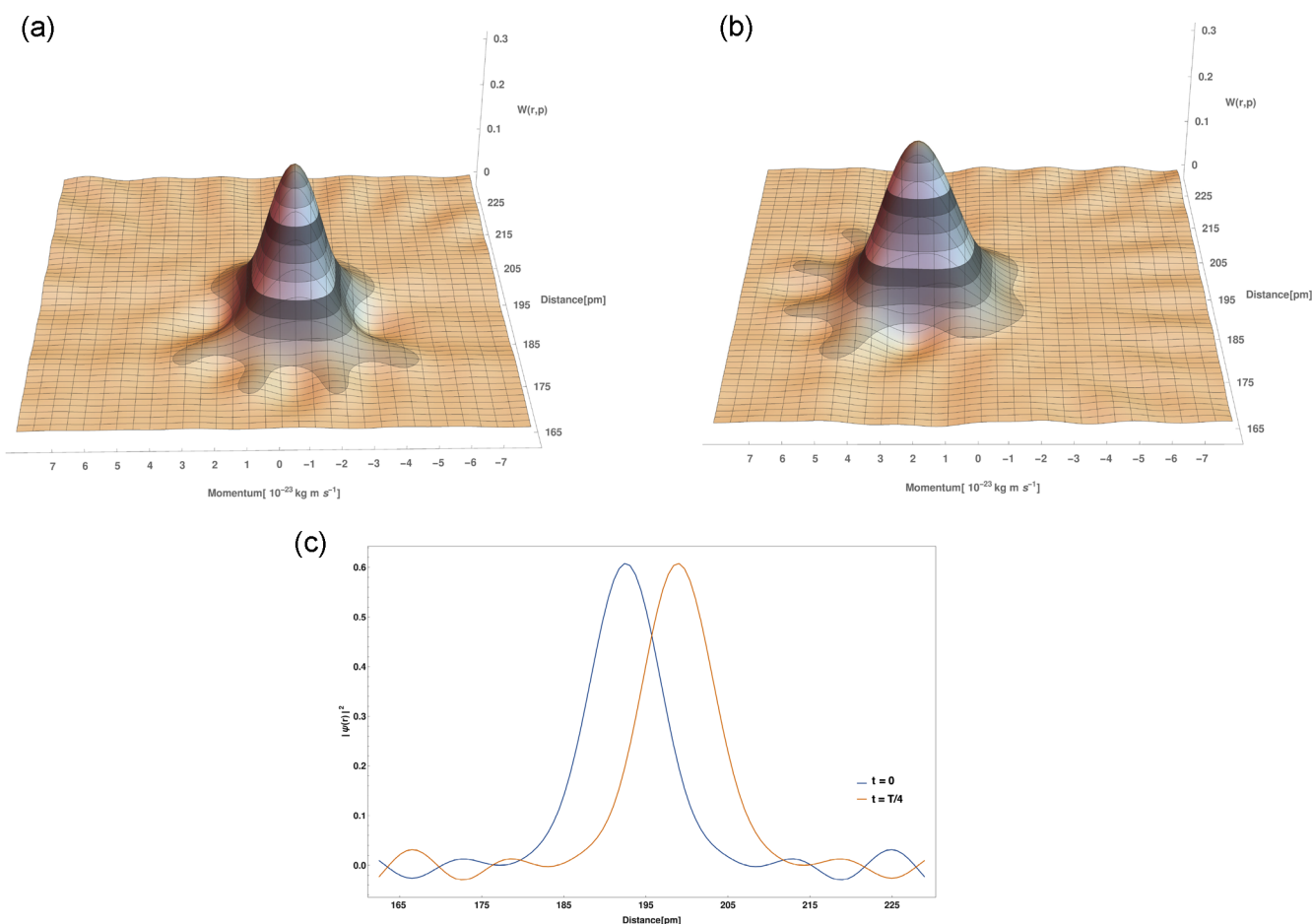
Figure 6. (a) Wigner function for CH_3Br at $t = 0$, calculated by an inverse radon transformation of the nuclear probability density obtained from the simulated wavepacket dynamics. (b) Temporal evolution of Wigner Function, plotted at $t = T/4$. (c) Nuclear probability densities reconstructed from corresponding Wigner functions at (b) $t = 0$ and (c) $t = T/4$, respectively.

context or rather challenge we now present a model system. We simulated the dynamics of a coherent vibrational wavepacket of CH_3Br on its electronic ground state, which can be created through strong field process.[155,156] The nuclear probability density of the wave packet is shown in Figure 5a as a function of time t and internuclear distance r of the C−Br atom pair. The wave packet oscillates with a period of 55.1 fs.

The gas phase electron scattering intensity corresponding to this wavepacket is shown in Figure 5b, defined as a function of time t and magnitude of momentum transfers.

The momentum transfer vector $\mathbf{s}$ is defined by its magnitude, $s = 4\pi \sin(\theta/2)/\lambda$, and angle φ relative to x-axis of the detector plane. The modified molecular intensity $sM(\mathbf{s})$ is used to reveal the details of the scattering signal,

$$sM(\mathbf{s}) = s\frac{I_M(\mathbf{s})}{I_A(s)} \tag{11}$$

where the molecular intensity $I_M(s)$ summed over all atom pairs and $I_A(s)$ summed over all atoms. For the purpose of modeling the $I_M(s)$ was calculated in the following simplified form[18]

$$I_M(\mathbf{s}) = \left\{ \sum_{i \neq j} g_{ij}(s) e^{-l_{ij}^2 s^2/2} F_{ij}(\mathbf{s}) \right\}_{r_{ij} \neq r_{C-Br}} + \left\{ g(s) \int dr P(r) F(\mathbf{s}) \right\}_{r_{ij} = r_{C-Br}}$$

$$I_A(s) = \sum_i |f_i|^2 \tag{12}$$

where f, r and η_i are defined as above and l_{ij} is the RMS amplitude of vibration for atoms i and j. These were estimated using a harmonic frequency calculation in combination with the program SHRINK. $F_{ij}(\mathbf{s})$ is the integral $\int d\mathbf{r}_{ij} d\mathbf{p}_{ij} W(\mathbf{r}_{ij}, \mathbf{p}_{ij}, t) \exp(i\mathbf{s}\mathbf{r}_{ij})$ for a rigid molecule over all orientational degrees of freedom and depends upon the specific molecular alignment distribution. We define a spatial distribution of orientations of the atomic pairs r_{ij} using a $\cos^2 \phi$ probability function, where ϕ is the angle between the transition dipole and the laser polarization. In CH_3Br, the transition dipole axis is parallel to $\mathbf{r}_{C-Br}$ and defines an angle Ω_{ij} with each atomic pair. Taking a spatial distribution for excitation perpendicular to the electron beam, $F_{ij}(\mathbf{s})$ takes the form,

$$F_{ij}(\mathbf{s}) = \frac{j_1(sr_{ij})}{sr_{ij}} - \sin^2 \Omega_{ij} + (2 - 3\sin^2 \Omega_{ij})\cos^2(\theta/2)\cos^2 \varphi \frac{j_2(sr_{ij})}{2} \tag{13}$$

where $j_k(x)$ is the kth order spherical Bessel function.[157−159] The change in the structure of CH_3Br, as the internuclear distance between C−Br increases, is accommodated by referencing the geometrical structure of the molecule. We plot the simulated diffraction intensity $sM(\mathbf{s}, t)$ for $t = 0$ and $t = T/2$, with T being the vibrational period, in Figure 5c and d, respectively. In Figure 5e, we show a plot of the difference of the simulated diffraction patterns between $t = T/2$ and $t = 0$.

We use inverse Radon Transformation to reconstruct the Wigner function in terms of a tomographic projection $Pr(r, t)$.

$$W(r, p) = \frac{1}{2\pi^2} \int_{-\infty}^{\infty} dx \int_{0}^{\pi} d\theta Pr(x, \theta)K(r\cos\theta + p\sin\theta - x)$$

(14)

where $K(x) = \frac{1}{2} \int_{-\infty}^{\infty} d\xi |\xi| e^{-i\xi x}$ is the kernel of the Radon transformation, where x, r are unitless coordinates and p is the unitless momentum, and $\theta = \omega t$.

The Wigner function is constructed for the simulated wavepacket, as shown Figure 6a. Gaussian quadrature is used for the integration. The constructed Wigner function is used as an initial condition to construct the time evolution of the Wigner function at $t = T/4$, shown in Figure 6b. From the Wigner functions, nuclear probability densities can be faithfully reconstructed in Figure 6c.

We use the quantum tomographic method to reconstruct the density matrix ρ of the wavepacket. The density matrix elements ρ_{mn} can be expressed in terms of $Pr(r, t) = |\psi(r, t)|^2$, by the following formulation,

$$\rho_{mn} = \int dr \tilde{Pr}(r, \omega_m - \omega_n) f_{mn}(r)$$

(15)

where $\tilde{Pr}(r, \omega_m - \omega_n)$ is the Fourier transform of the time dependent probability density $Pr(r, t)$ and $f_{mn}(r)$ are the pattern functions.[157,158]

$$f_{mn}(r) = \frac{\partial[\Psi_m(r)\phi_n(r)]}{\partial r}$$

(16)

where $\Psi_m(r)$ and $\phi_n(r)$ are the normalized regular and non-normalizable irregular wave function of the Schrödinger equation.[157−159] The calculated pattern functions $f_{mn}(r)$ for the first three vibrational levels are depicted in Figure 7a. Gaussian quadrature for the integration is used for the integration. The modulus of the density matrix elements are plotted for the first five vibrational levels (see Figure 7b).

SPATIAL, TEMPORAL RESOLUTION FOR QUANTUM TOMOGRAPHY AND STATISTICAL ERROR IN RECONSTRUCTION OF DENSITY MATRIX

Reconstructing the density matrix up to Nth order requires certain spatial and temporal resolution. The pattern function can be approximated around $x = 0$ as[160]

$$f_{nn}(x) \sim -2 \sin\left[-\pi\left(n + \frac{1}{2}\right) + 2\sqrt{n + 1}x\right]$$

(17)

where x is the unitless coordinate. In order to resolve a period of the oscillation of the pattern function that arises in the convolution (eq 15), the required spatial resolution for reconstructing density matrix up to Nth order has to be better than

$$\Delta x \leq \frac{1}{2} \frac{\pi}{\sqrt{2N + 1}}$$

(18)

The maximal order of the desired density matrix also sets demand on the temporal resolution. Suppose d time intervals are measured for a half a period of molecular vibration, we have a phase resolution of π/d for the Fourier transformation of probability distribution function in eq 15. The aliasing phenomena defines the maximal order of density matrix we
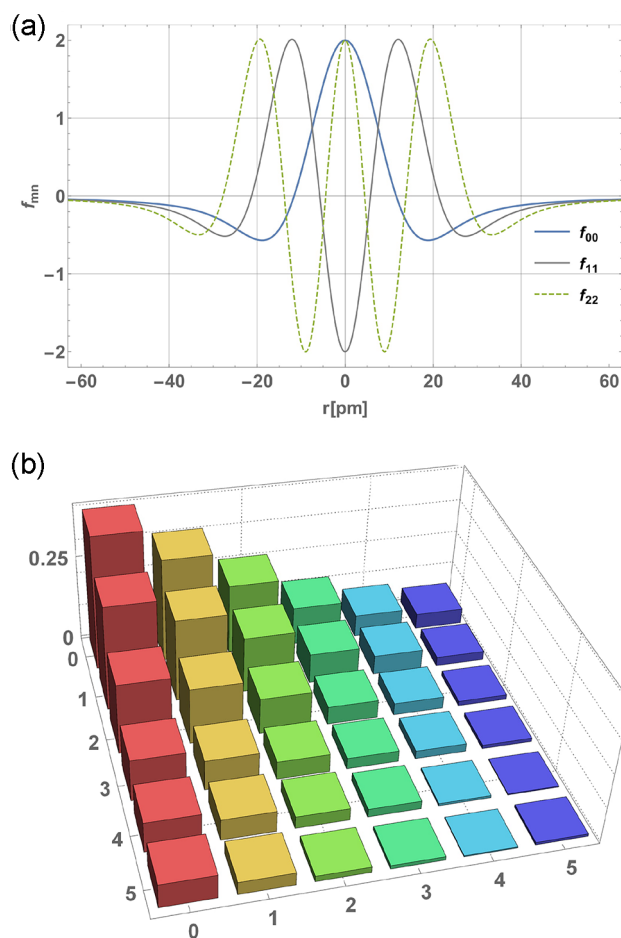

Figure 7. (a) Pattern functions for first three vibrational levels constructing the simulated vibrational wavepacket. (b) Modulus of density matrix, ρ_{mn}, obtained by tomographic reconstruction of the probability density graph yielded, provided by the simulated wave packet dynamics of CH_3Br on the electronic ground state.

can access to be $N = d - 1$,[161] thus, the required temporal resolution can be written as

$$\Delta t \leq \frac{T}{2(N + 1)}$$

(19)

where T is the period of the approximated harmonic oscillation of the molecule. Taken CH_3Br as an example, the spatial and temporal resolution required for reconstructing density matrix up to $N = 5$ is $\Delta r = 3.1$ pm and $\Delta t = 4.6$ fs, respectively. In other words, the spatial resolution has to be sufficient to directly resolve the nodes of the vibrational wavepacket, which is within reach by electron diffraction with a sufficient number of registered electrons.[30]

If we think about the feasibility of such an experiment, the temporal resolution is certainly challenging, but may be met by either novel relativistic sources,[95] compressed or streaking methods, or by making use of novel electron sources that have the prospect to go to the attosecond domain,[162−165] albeit with the same issues as low brightness sources. In terms of spatial resolution, this is more difficult to assess, since the electron wavelength itself (3.7 pm at 100 keV/0.87 pm at 1 MeV) should not limit the resolution and diffraction experiments typically yield geometrical parameters with precisions approaching 0.1 pm. However, care should be taken here as to exactly what we

mean by resolution, since quantum tomography requires knowledge of not just the mean positions and width of the distribution, but also the precise shape itself. If we assume that ultrafast electron diffraction would be able to equal gas-phase electron diffraction (GED) in terms of spatial resolution, we can eventually expect to record data out to a resolution of $s_{max} = 30-40$ Å^{-1}, which corresponds to a formal resolution of about 20 pm ($2\pi/s_{max}$), as generally defined in crystallography. However, this represents the minimum d-spacing that can be observed, and the resolution of a density map obtained from a full data set is about two times greater and would approximately correspond to the diffraction limit of the measurement ($\lambda/2 \sin \theta$), as defined by the electron wavelength and numerical aperture defined by s_{max}. However, given the sensitivity of GED to small structure changes, we expect it would be possible to obtain a probability distribution of nuclei from the diffraction data with significantly higher resolution, in combination with additional information such as the atomic scattering factors and assumptions such as smoothness and non-negativity of the probability distribution, in a similar vein to the methods employed in super-resolution microscopy. Returning to the experimental issues, the resolution is therefore not limited by the electron wavelength and detector size, but rather the counting statistics and the ability to distinguish elastically scattered electrons from background at wide scattering angles, and for crystal studies, the crystal quality also plays a significant role.

Since we can only take a finite number of samples at each time interval, the constructed density matrix elements must have statistical errors. Suppose N_t samples of nuclear probability distribution are taken per time interval, and the measurements follows Poissionian statistics, the measured probability distribution has a statistical variance $\sigma^2_{x,t}$ around the true value $Pr_{tr}(x, t)$

$$\sigma^2_{x,t} = \frac{\pi}{N_t} Pr_{tr}(x, t) \tag{20}$$

and the variance and error bar of each density matrix element can be calculated accordingly.[81] For the CH$_3$Br model system, we present the estimation of statistical errors in Figure 8.
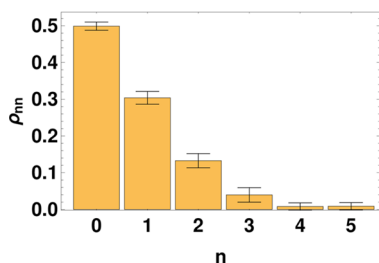

Figure 8. Estimation of statistical errors of diagonal density matrix elements, assuming that the probability distribution was measured with 100 samples per time interval and the measurements follow Poissonian statistics.

EXTENDING BEYOND ONE-DIMENSIONAL DYNAMICS

Quantum tomographic reconstruction provides access to measuring molecular states, in the form of the Wigner function and density matrix, with the temporal evolution of nuclei and electron probability density $Pr(r, t)$ measured by ultrafast diffraction. Significant theoretical and experimental research has

been focused on quantum tomography methods; however, the existing approaches cannot be used beyond the one-dimensional case. Since, in most cases, molecular dynamics involve dimensions much higher than one, this so-called "dimension problem" obstructs any attempt of a realistic application of quantum state tomography.[166,167] To be precise, for vibrational state tomography, only diatomic molecules and molecules that have effectively a single dominant vibrational mode allow complete tomographic reconstruction of their quantum states. Because for a molecule with N vibrational modes, its density matrix has dimension of $2N$, to reconstruct the $2N$ dimensional density matrix from the $(N + 1)$-dimensional nuclear probability density $Pr(r_1, ..., r_N; t)$, a nonsingular transformation matrix can only exist for $N = 1$. Thus, the vibrational states tomography from ultrafast diffraction is seemingly limited to diatomic molecules with only one vibrational mode. For the rotational states, quantum tomography by means of diffraction, in its current form, would even fail for the simplest diatomic molecule, because its full quantum state $\langle \theta, \phi | \hat{\rho} | \theta', \phi' \rangle$ has four degrees of freedom, which is of higher dimension than the measurable 3D nuclear probability density $Pr(\theta, \phi, t)$. Fortunately, even with the limitation due to dimension problem of rotational states quantum tomography, the quantum states of 1D vibrational motion can be faithfully extracted from ultrafast diffraction, because the molecular dynamical trajectory is encoded in pair distribution functions (PDF) of atom pairs of molecule,[111] which essentially reflect the dynamics in terms of internal vibrational coordinates that are independent of the overall rotational and translational motion.

To alleviate the obstructive dimension problem, we can establish a connection between molecular quantum tomography and the phase retrieval techniques, which lie at the heart of many X-ray and electron imaging methods, such as crystallography, coherent diffraction imaging and ptychography.[168] With the diagram in Figure 9, we present the analogous connection
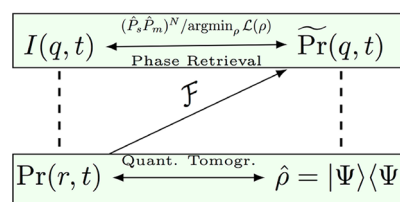

Figure 9. Analogous connection between phase retrieval and quantum tomography. $I(q,t)$ is diffraction intensity in reciprocal space with momentum transfer q, $Pr(r, t) = |\Psi(r, t)|^2$ is the nuclear probability density, and $\hat{\rho} = |\Psi\rangle\langle\Psi|$ is density matrix operator of a pure state (the generalization to mixed states is trivial). To reconstruct the complex wave function $\Psi(r, t)$ from the real nuclear probability density $Pr(r, t)$ can be made mathematically equivalent to phase retrieval.

between the two pairs of physical quantities, $(I, Pr(r))$ of diffraction imaging and $\widetilde{Pr}(q)$, $\hat{\rho}$ of quantum state tomography. Especially, the measured diffraction intensity $I(q)$ also has lower dimension than the Fourier transformed probability density of nuclei or electrons $\widetilde{Pr}(q) = \mathcal{F}[Pr(r)]$ in reciprocal space, which is known as the "phase problem" in diffraction imaging, and the central task of phase retrieval procedure is to recover the higher dimensional object $\widetilde{Pr}(q)$ by adding intuitive physical conditions.[169] The view of quantum tomography as a phase retrieval problem can date back to Pauli's original formulation in

Handbook of Physics:[170] "These functions $\Psi(x, t)$ and $\phi(p)$ are, with regard to their phase, not directly observable; this is rather for the probability densities $W(x)$ and $W(p)$. The mathematical question, whether the wave function Ψ can always be explicitly determined through given function of $W(x)$ and $W(p)$, is not yet generally investigated." In reply to this central question of quantum tomography, it was proven by Feenberg that the reconstruction of 1D wave function $\Psi(x, t)$ with its phase can be made from knowing the unitary evolution of the probability density $W(x, \theta) = |\Psi(x, \theta)|^2$ parametrized by θ.[145] In the case of quantum tomography by ultrafast diffraction, the role of the unitary evolution parameter θ is naturally played by the time t.

A direct attempt to treat quantum tomography beyond 1D employing its analogue with phase retrieval problem, is to use the iterative projection methods developed for crystallography and coherent diffraction imaging.[145] The basis of the algorithm is to find the intersection between the two sets for quantum tomography: the set of all objects with given probability density $\Pr(r, t)$ (modulus set, M) and the set of all the objects that are within a given area of support volume (positive support set, S). When the reconstructed density matrix of quantum states belongs to both sets simultaneously, a solution is reached. Such a treatment can have mathematically provable convergence.[169] Precisely, in the case of rotational state tomography, the modulus set is reconstructed in each iteration through a probability projector $\hat{P}_m = \mathcal{F}^{-1}\hat{P}_m\mathcal{F}$ operating on the nuclear probability density $\Pr(r, t)$, where the operator $\hat{P}_m$ replaces the modulus of density matrix element $|\rho_{JM, JM}|$ with that from measurements, and keep the phase inherited from iterative procedure. Next, the $\hat{P}_s$ operator in turn projects out the unphysical values of $\hat{P}_m[\Pr(r, t)]$ for all time that corresponds to negative probability density of nuclei, or projects to a support set with more restrictions from physical intuition. It was proved that the algorithms comprised of alternative projections $(\hat{P}_s\hat{P}_m)^M$ are equivalent to the minimization of distance $d(\Pr) = \|\hat{P}_m\Pr - \hat{P}_s\Pr\|^2$ with the steepest descent of Gaussian likelihood.[169] And several modified variations incorporating the reflection operator $\hat{R} = \hat{I} - 2[\hat{P} - \hat{I}]$ can solve this minimization problem with higher efficiency.[168]

An alternative method can be devised based on the Bayesian probability theory, since it has been shown to be powerful in solving phase retrieval problems, even under low dose illumination condition.[171] By its mathematical nature, the phase problem can be reformulated in terms of Bayesian inference problem, and its analogue in quantum tomography can be similarly treated by nonconvex optimization of the object function for the maximum-a-posteriori (MAP) estimate:

$$\rho_{\text{MAP}} = \arg\min_\rho \mathcal{L}_{\text{MAP}}(\rho) = \arg\min_\rho\left[-\log\left(\frac{P(PR|\rho)P(\rho)}{P(\Pr)}\right)\right] \quad (21)$$

to infer the density matrix ρ from the nuclear probability density $\Pr(r, t)$ obtained from ultrafast diffraction. There are various candidates to define the MAP object function $\mathcal{L}_{\text{MAP}}(\rho)$, for example, from the BM3D collaborative filtering algorithm,[171] and nonconvex algorithms that can provably converge to a global minimum with suitable initialization.[169]

■ CONCLUDING REMARKS

We have presented the current state of the art in imaging chemistry. From a chemical perspective, the fundamental space-time limit to imaging relative atomic motions has been achieved.

This atomic level of detail has revealed the key reaction modes directing chemistry that ultimately is the simple physics we were missing to understand the transferability of chemistry to arbitrarily complex systems up to the scale of biological systems. We can now combine both structure and dynamics in a unifying way through conceptualizing chemistry through the displacement of the key reaction modes to better define the critical point or transition state region. The new conceptual basis that is emerging from this field will greatly advance our chemical intuition in how to control barrier heights and thereby chemistry. This new insight may well enable chemistry to scale to the control of molecular problems on the level of true biomimics. As with all things, the higher and higher level of resolution to observing natural phenomena, the higher the level of understanding. This atomic level of imaging chemistry will certainly advance our understanding of chemical reaction mechanisms and level of control.

The other important point, we have emphasized is that we are losing the quantum aspects of the problem by reverting to classical depictions of ensemble averaged atomic positions, even in mapping out the dynamics. To access the quantum information that is currently hidden, we have presented the theory of quantum tomographic reconstruction of molecular quantum states by ultrafast diffraction, and presented the ultimate demands for imaging resolution in spatial and temporal domains depending on the complexity of quantum coherence of the vibrational, rotational and electronic states. We have also pointed out potential routes toward overcoming the dimension problem. It is a grand challenge to capture the electronic coherence and effect on nuclear probability distributions when a molecular wave packet passes through a conical intersection, or other chemically relevant transitions, by means of ultrafast spectroscopy and diffraction.[172,173] Although the interference terms cannot appear directly in the differential cross section of elastic scattering,[173−175] but the coherence could eventually be revealed via the quantum tomographically reconstructed Wigner function and density matrix. In this sense, ultrafast diffraction not only provides us with a molecular movie, but holds the promise to give nearly complete information on the molecule as a quantum system.

While the spatial resolution required is challenging to accessing quantum information on chemical passage, there does not seem to be any hard physical limits to prevent it being achieved. Electrons with an energy of 100 keV have a wavelength of 3.4 pm, thus a diffraction limit of <3 pm is theoretically obtainable, but substantially beyond what is typically achieved even in ground-state diffraction experiments. The main problem stems from the rapid decay of the elastic scattering, which falls with $1/s^4$, leading to low counting statistics and an over-shadowing of the elastic scattering by various background sources such as inelastic scattering, and secondary electrons, which begin to dominate the signal at a resolution of about 10 pm. However, application of super-resolution techniques or energy-resolved detectors may bring this within reach. The temporal resolution required is similarly challenging, but not beyond the realm of possibility, probably requiring pulse compression or streaking techniques reaching the few-femto-second regime. With our current atomic vision of chemical processes, the question is whether we can see beyond to the quantum conditions on the structural transitions. We present this quantum problem in image reconstruction of chemistry as the next major challenge for both experimental and theoretical

camps in ultrafast diffraction, to make waves in our understanding of chemistry.

■ AUTHOR INFORMATION

Corresponding Author

*E-mail: dwayne.miller@mpsd.mpg.de.

ORCID ◉

Zheng Li: 0000-0002-5483-9149

R. J. Dwayne Miller: 0000-0003-0884-0541

Author Contributions

#These authors contributed equally to this work.

Notes

The authors declare no competing financial interest.

■ REFERENCES

(1) Manfred Eigen Immeasurably Fast Reactions. *Nobel Lecture*, 1967.

(2) Arrhenius, S. Über die Dissociationswärme und den Einfluss der Temperatur auf den Dissociationsgrad der Elektrolyte. *Z. Phys. Chem.* **1889**, *4*, 96.

(3) Atkins, P. W.; de Paula, J. *Physical Chemistry*; Oxford University Press, 2017.

(4) Dwyer, J. R.; Hebeisen, C. T.; Ernstorfer, R.; Harb, M.; Deyirmenjian, V. B.; Jordan, R. E.; Dwayne Miller, R. Femtosecond electron diffraction - 'making the molecular movie'. *Philos. Trans. R. Soc., A* **2006**, *364*, 741.

(5) Sciaini, G.; Miller, R. D. Femtosecond electron diffraction - heralding the era of atomically resolved dynamics. *Rep. Prog. Phys.* **2011**, *74*, No. 096101.

(6) Stankus, B.; Budarz, J. M.; Kirrander, A.; Rogers, D.; Robinson, J.; Lane, T. J.; Ratner, D.; Hastings, J.; Minitti, M. P.; Weber, P. M. Femtosecond photodissociation dynamics of 1, 4-diiodobenzene by gas-phase X-ray scattering and photoelectron spectroscopy. *Faraday Discuss.* **2016**, *194*, 525.

(7) Wang, Q.; Schoenlein, R. W.; Peteanu, L. A.; Mathies, R. A.; Shank, C. V. Vibrationally coherent photochemistry in the femtosecond primary event of vision. *Science* **1994**, *266*, 422.

(8) Johnson, P. J.; Farag, M. H.; Halpin, A.; Morizumi, T.; Prokhorenko, V. I.; Knoester, J.; Jansen, T. L.; Ernst, O. P.; Miller, R. D. The primary photochemistry of vision occurs at the molecular speed limit. *J. Phys. Chem. B* **2017**, *121*, 4040.

(9) Johnson, P. J.; Halpin, A.; Morizumi, T.; Brown, L. S.; Prokhorenko, V. I.; Ernst, O. P.; Miller, R. J. D. The photocycle and ultrafast vibrational dynamics of bacteriorhodopsin in lipid nanodiscs. *Phys. Chem. Chem. Phys.* **2014**, *16*, 21310.

(10) Marcus, R. A.; Sutin, N. Electron transfers in chemistry and biology. *Biochim. Biophys. Acta, Rev. Bioenerg.* **1985**, *811*, 265.

(11) Maroncelli, M.; MacInnis, J.; Fleming, G. R. Polar solvent dynamics and electron-transfer reactions. *Science* **1989**, *243*, 1674.

(12) Yoshihara, K.; Tominaga, K.; Nagasawa, Y. Effects of the solvent dynamics and vibrational motions in electron transfer. *Bull. Chem. Soc. Jpn.* **1995**, *68*, 696.

(13) Kosower, E. M.; Huppert, D. Excited state electron and proton transfers. *Annu. Rev. Phys. Chem.* **1986**, *37*, 127.

(14) Barbara, P. F.; Walker, G. C.; Smith, T. P. Vibrational modes and the dynamic solvent effect in electron and proton transfer. *Science* **1992**, *256*, 975.

(15) Jean-Ruel, H.; Gao, M.; Kochman, M. A.; Lu, C.; Liu, L. C.; Cooney, R. R.; Morrison, C. A.; Miller, R. D. Ring-closing reaction in diarylethene captured by femtosecond electron crystallography. *J. Phys. Chem. B* **2013**, *117*, 15894.

(16) Das, A.; Mandal, I.; Venkatramani, R.; Dasgupta, J. Ultrafast photoactivation of C−H bonds inside water-soluble nanocages. *Science Adv.* **2019**, *5*, No. eaav4806.

(17) Heitele, H. Dynamic Solvent Effects on Electron-Transfer Reactions. *Angew. Chem., Int. Ed. Engl.* **1993**, *32*, 359.

(18) Hynes, J. T. Molecules in motion: chemical reaction and allied dynamics in solution and elsewhere. *Annu. Rev. Phys. Chem.* **2015**, *66*, 1.

(19) Orr-Ewing, A. J. Taking the plunge: chemical reaction dynamics in liquids. *Chem. Soc. Rev.* **2017**, *46*, 7597.

(20) McQuarrie, D. A. *Statistical Mechanics*; University Science Books, 2000.

(21) Worth, G. A.; Cederbaum, L. S. Beyond Born-Oppenheimer - molecular dynamics through a conical intersection. *Annu. Rev. Phys. Chem.* **2004**, *55*, 127.

(22) Worth, G. A.; Cederbaum, L. S. Beyond Born-Oppenheimer: molecular dynamics through a conical intersection. *Annu. Rev. Phys. Chem.* **2004**, *55*, 127.

(23) de la Escosura, A.; Martínez-Díaz, M. V.; Guldi, D. M.; Torres, T. Stabilization of Charge-Separated States in Phthalocyanine− Fullerene Ensembles through Supramolecular Donor− Acceptor Interactions. *J. Am. Chem. Soc.* **2006**, *128*, 4112.

(24) Miller, R. J. D.; Nozik, A.; McLendon, G.; Schmickler, W.; Willig, F. *Surface Electron Transfer Processes*; John Wiley & Sons, 1995.

(25) Marcus, R. A. Electron transfer reactions in chemistry. Theory and experiment. *Rev. Mod. Phys.* **1993**, *65*, 599.

(26) Newton, M. D.; Sutin, N. Electron transfer reactions in condensed phases. *Annu. Rev. Phys. Chem.* **1984**, *35*, 437.

(27) Kubař, T.; Elstner, M. What governs the charge transfer? The role of conformation and environment. *J. Phys. Chem. B* **2008**, *112*, 8788.

(28) Kubař, T.; Elstner, M. A hybrid approach to simulation of electron transfer in complex molecular systems. *J. R. Soc., Interface* **2013**, *10*, 20130415.

(29) Oberhofer, H.; Blumberger, J. Charge constrained density functional molecular dynamics for simulation of condensed phase electron transfer reactions. *J. Chem. Phys.* **2009**, *131*, No. 064101.

(30) Ischenko, A. A.; Kochikov, I. V.; Miller, R. J. D. The effect of Coulomb repulsion on the space-time resolution limits for ultrafast electron diffraction. *J. Chem. Phys.* **2019**, *150*, No. 054201.

(31) Ischenko, A. A.; Weber, P. M.; Miller, R. J. D. Capturing chemistry in action with electrons: realization of atomically resolved reaction dynamics. *Chem. Rev.* **2017**, *117*, 11066.

(32) Turner, A. R.; Robertson, H. E.; Borisenko, K. B.; Rankin, D. W.; Fox, M. A. Gas-phase electron diffraction studies of the icosahedral carboranes, ortho-, meta-and para-C 2 B 10 H 12. *Dalton Transactions* **2005**, 1310.

(33) Mackie, I. D.; Robertson, H. E.; Rankin, D. W.; Fox, M. A.; Malget, J. M. Gas-Phase Electron Diffraction Studies on Two 11-Vertex Dicarbaboranes, closo-2, 3-C2B9H11 and nido-2, 9-C2B9H13. *Inorg. Chem.* **2004**, *43*, 5387.

(34) Miller, R. J. D. Mapping Atomic Motions with Ultrabright Electrons - The Chemists' Gedanken Experiment Enters the Lab Frame. *Annu. Rev. Phys. Chem.* **2014**, *65*, 583.

(35) Miller, R. D. Femtosecond crystallography with ultrabright electrons and x-rays: Capturing chemistry in action. *Science* **2014**, *343*, 1108.

(36) Bargheer, M.; Zhavoronkov, N.; Gritsai, Y.; Woo, J.; Kim, D.; Wörner, M.; Elsässer, T. Coherent atomic motions in a nanostructure studied by femtosecond X-ray diffraction. *Science* **2004**, *306*, 1771.

(37) Nie, S.; Wang, X.; Park, H.; Clinite, R.; Cao, J. Measurement of the Electronic Gr\"uneisen Constant Using Femtosecond Electron Diffraction. *Phys. Rev. Lett.* **2006**, *96*, No. 025901.

(38) Cavalleri, A.; Siders, C. W.; Brown, F. L. H.; Leitner, D. M.; Tóth, C.; Squier, J. A.; Barty, C. P. J.; Wilson, K. R.; Sokolowski-Tinten, K.; Horn von Hoegen, M.; von der Linde, D.; Kammler, M. Anharmonic Lattice Dynamics in Germanium Measured with Ultrafast X-Ray Diffraction. *Phys. Rev. Lett.* **2000**, *85*, 586.

(39) Rose-Petruck, C.; Jimenez, R.; Guo, T.; Cavalleri, A.; Siders, C. W.; Rksi, F.; Squier, J. A.; Walker, B. C.; Wilson, K. R.; Barty, C. P. Picosecond−milliångström lattice dynamics measured by ultrafast X-ray diffraction. *Nature* **1999**, *398*, 310.

(40) Born, M.; Wolf, E. *Principles of Optics: Electromagnetic Theory of Propagation, Interference and Diffraction of Light*; Elsevier, 2013.

(41) Goodhew, P. J.; Humphreys, J.; Beanland, R. *Electron Microscopy and Analysis*; CRC Press, 2000.

(42) Shih, Y. *An Introduction to Quantum Optics: Photon and Biphoton Physics*; CRC Press, 2018.

(43) Shih, Y. In *Classical, Semi-classical and Quantum Noise*; Cohen, L., Poor, V., Scully, M., Eds.; Springer, 2012; p 169.

(44) Chapman, H. N.; Nugent, K. A Coherent lensless X-ray imaging. *Nat. Photonics* **2010**, *4*, 833.

(45) Guss, J. M.; Merritt, E. A.; Phizackerley, R. P.; Hedman, B.; Murata, M.; Hodgson, K. O.; Freeman, H. C. Phase determination by multiple-wavelength x-ray diffraction: crystal structure of a basic″ blue″ copper protein from cucumbers. *Science* **1988**, *241*, 806.

(46) Hendrickson, W. A.; Pähler, A.; Smith, J. L.; Satow, Y.; Merritt, E. A.; Phizackerley, R. P. Crystal structure of core streptavidin determined from multiwavelength anomalous diffraction of synchrotron radiation. *Proc. Natl. Acad. Sci. U. S. A.* **1989**, *86*, 2190.

(47) Hendrickson, W. A. Determination of macromolecular structures from anomalous diffraction of synchrotron radiation. *Science* **1991**, *254*, 51.

(48) Son, S.-K.; Chapman, H. N.; Santra, R. Multiwavelength anomalous diffraction at high X-ray intensity. *Phys. Rev. Lett.* **2011**, *107*, 218102.

(49) Spence, J. C.; Doak, R. B. Single molecule diffraction. *Phys. Rev. Lett.* **2004**, *92*, 198102.

(50) Henderson, R. The potential and limitations of neutrons, electrons and X-rays for atomic resolution microscopy of unstained biological molecules. *Q. Rev. Biophys.* **1995**, *28*, 171.

(51) Neutze, R.; Wouts, R.; van der Spoel, D.; Weckert, E.; Hajdu, J. Potential for biomolecular imaging with femtosecond X-ray pulses. *Nature* **2000**, *406*, 752.

(52) Quiney, H. M.; Nugent, K. A. Biomolecular imaging and electronic damage using X-ray free-electron lasers. *Nat. Phys.* **2011**, *7*, 142.

(53) Armstrong, M. R.; Reed, B. W.; Torralva, B. R.; Browning, N. D. Prospects for electron imaging with ultrafast time resolution. *Appl. Phys. Lett.* **2007**, *90*, 114101.

(54) Reed, B.; Armstrong, M.; Browning, N.; Campbell, G.; Evans, J.; LaGrange, T.; Masiel, D. The evolution of ultrafast electron microscope instrumentation. *Microsc. Microanal.* **2009**, *15*, 272.

(55) Lobastov, V. A.; Srinivasan, R.; Zewail, A. H. Four-dimensional ultrafast electron microscopy. *Proc. Natl. Acad. Sci. U. S. A.* **2005**, *102*, 7069.

(56) Bainbridge, A.; Barlow Myers, C.; Bryan, W. Femtosecond few-to-single-electron point-projection microscopy for nanoscale dynamic imaging. *Struct. Dyn.* **2016**, *3*, No. 023612.

(57) Flannigan, D. J.; Zewail, A. H. 4D electron microscopy: principles and applications. *Acc. Chem. Res.* **2012**, *45*, 1828.

(58) Shorokhov, D.; Zewail, A. H. Perspective: 4D ultrafast electron microscopy—Evolutions and revolutions. *J. Chem. Phys.* **2016**, *144*, No. 080901.

(59) Glaeser, R. M. How Good Can Single-Particle Cryo-EM Become? What Remains Before It Approaches Its Physical Limits? *Annu. Rev. Biophys.* **2019**, *48*, 45.

(60) Mueller, C.; Harb, M.; Dwyer, J.; Miller, R. D. Nanofluidic cells with controlled pathlength and liquid flow for rapid, high-resolution in situ imaging with electrons. *J. Phys. Chem. Lett.* **2013**, *4*, 2339.

(61) Keskin, S.; Besztejan, S.; Kassier, G. n.; Manz, S.; Bücker, R.; Riekeberg, S.; Trieu, H. K.; Rentmeister, A.; Miller, R. D. Visualization of multimerization and self-assembly of DNA-functionalized gold nanoparticles using in-liquid transmission electron microscopy. *J. Phys. Chem. Lett.* **2015**, *6*, 4487.

(62) Fu, X.; Chen, B.; Tang, J.; Hassan, M. T.; Zewail, A. H. Imaging rotational dynamics of nanoparticles in liquid by 4D electron microscopy. *Science* **2017**, *355*, 494.

(63) de Jonge, N. Theory of the spatial resolution of (scanning) transmission electron microscopy in liquid water or ice layers. *Ultramicroscopy* **2018**, *187*, 113.

(64) Engelen, W.; Van Der Heijden, M.; Bakker, D.; Vredenbregt, E.; Luiten, O. High-coherence electron bunches produced by femtosecond photoionization. *Nat. Commun.* **2013**, *4*, 1693.

(65) McCulloch, A.; Sheludko, D.; Junker, M.; Scholten, R. High-coherence picosecond electron bunches from cold atoms. *Nat. Commun.* **2013**, *4*, 1692.

(66) Lee, C.; Tsujino, S.; Miller, R. D. Transmission low-energy electron diffraction using double-gated single nanotip field emitter. *Appl. Phys. Lett.* **2018**, *113*, No. 013505.

(67) Baum, P. On the physics of ultrashort single-electron pulses for time-resolved diffraction. *Chem. Phys.* **2013**, *423*, 55.

(68) Chapman, H. N.; Barty, A.; Bogan, M. J.; Boutet, S.; Frank, M.; Hau-Riege, S. P.; Marchesini, S.; Woods, B. W.; Bajt, S.; Benner, W. H.; et al. Femtosecond diffractive imaging with a soft-X-ray free-electron laser. *Nat. Phys.* **2006**, *2*, 839.

(69) Chapman, H. N.; Fromme, P.; Barty, A.; White, T. A.; Kirian, R. A.; Aquila, A.; Hunter, M. S.; Schulz, J.; DePonte, D. P.; Weierstall, U.; et al. Femtosecond X-ray protein nanocrystallography. *Nature* **2011**, *470*, 73.

(70) Siwick, B. J.; Dwyer, J. R.; Jordan, R. E.; Miller, R. D. An atomic-level view of melting using femtosecond electron diffraction. *Science* **2003**, *302*, 1382.

(71) Siwick, B. J.; Dwyer, J. R.; Jordan, R. E.; Miller, R. J. D. Ultrafast electron optics - Propagation dynamics of femtosecond electron packets. *J. Appl. Phys.* **2002**, *92*, 1643.

(72) Siwick, B. J.; Dwyer, J. R.; Jordan, R. E.; Miller, R. J. D. Response to "Comment on 'Ultrafast electron optics - Propagation dynamics of femtosecond electron packets". *J. Appl. Phys.* **2003**, *94*, 807.

(73) Siwick, B. J.; Dwyer, J. R.; Jordan, R. E.; Miller, R. J. D. Femtosecond electron diffraction studies of strongly driven structural phase transitions. *Chem. Phys.* **2004**, *299*, 285.

(74) Floettmann, K. Generation of Sub-Fs Electron Beams at Few-MeV Energies. *Nucl. Instrum. Methods Phys. Res., Sect. A* **2014**, *740*, 34.

(75) van Oudheusden, T.; de Jong, E. F.; van der Geer, S. B.; Op't Root, W. P. E. M.; Luiten, O. J.; Siwick, B. J. Electron Source Concept for Single-Shot Sub-100 Fs Electron Diffraction in the 100 keV Range. *J. Appl. Phys.* **2007**, *102*, No. 093501.

(76) van Oudheusden, T.; Pasmans, P. L. E. M.; van der Geer, S. B.; de Loos, M. J.; van der Wiel, M. J.; Luiten, O. J. Compression of Subrelativistic Space-Charge-Dominated Electron Bunches for Single-Shot Femtosecond Electron Diffraction. *Phys. Rev. Lett.* **2010**, *105*, 264801.

(77) Gao, M.; Jean-Ruel, H.; Cooney, R. R.; Stampe, J.; de Jong, M.; Harb, M.; Sciaini, G.; Moriena, G.; Miller, R. J. D. Full characterization of RF compressed femtosecond electron pulses using ponderomotive scattering. *Opt. Express* **2012**, *20*, 12048.

(78) Gao, M.; Jiang, Y.; Kassier, G. H.; Dwayne Miller, R. Single shot time stamping of ultrabright radio frequency compressed electron pulses. *Appl. Phys. Lett.* **2013**, *103*, No. 033503.

(79) Otto, M. R.; René de Cotret, L.; Stern, M. J.; Siwick, B. J. Solving the jitter problem in microwave compressed ultrafast electron diffraction instruments: Robust sub-50 fs cavity-laser phase stabilization. *Struct. Dyn.* **2017**, *4*, No. 051101.

(80) Harb, M.; Ernstorfer, R.; Hebeisen, C. T.; Sciaini, G.; Peng, W.; Dartigalongue, T.; Eriksson, M. A.; Lagally, M. G.; Kruglik, S. G.; Miller, R. J. D. Electronically Driven Structure Changes of Si Captured by Femtosecond Electron Diffraction. *Phys. Rev. Lett.* **2008**, *100*, 155504.

(81) Gao, M.; Lu, C.; Jean-Ruel, H.; Liu, L. C.; Marx, A.; Onda, K.; Koshihara, S.-y.; Nakano, Y.; Shao, X.; Hiramatsu, T.; et al. Mapping molecular motions leading to charge delocalization with ultrabright electrons. *Nature* **2013**, *496*, 343.

(82) Ishikawa, T.; Hayes, S. A.; Keskin, S.; Corthey, G.; Hada, M.; Pichugin, K.; Marx, A.; Hirscht, J.; Shionuma, K.; Onda, K.; et al. Direct

observation of collective modes coupled to molecular orbital—driven charge transfer. *Science* **2015**, *350*, 1501.

(83) Otto, M. R.; de Cotret, L. P. R.; Valverde-Chavez, D. A.; Tiwari, K. L.; Émond, N.; Chaker, M.; Cooke, D. G.; Siwick, B. J. How optical excitation controls the structure and properties of vanadium dioxide. *Proc. Natl. Acad. Sci. U. S. A.* **2019**, *116*, 450.

(84) Chatelain, R. P.; Morrison, V. R.; Klarenaar, B. L.; Siwick, B. J. Coherent and incoherent electron-phonon coupling in graphite observed with radio-frequency compressed ultrafast electron diffraction. *Phys. Rev. Lett.* **2014**, *113*, 235502.

(85) Waldecker, L.; Bertoni, R.; Ernstorfer, R. Compact femtosecond electron diffractometer with 100 keV electron bunches approaching the single-electron pulse duration limit. *J. Appl. Phys.* **2015**, *117*, No. 044903.

(86) Gerbig, C.; Senftleben, A.; Morgenstern, S.; Sarpe, C.; Baumert, T. Spatio-temporal resolution studies on a highly compact ultrafast electron diffractometer. *New J. Phys.* **2015**, *17*, No. 043050.

(87) Hada, M.; Yamaguchi, D.; Ishikawa, T.; Sawa, T.; Tsuruta, K.; Ishikawa, K.; Koshihara, S.-y.; Hayashi, Y.; Kato, T. Ultrafast isomerization-induced cooperative motions to higher molecular orientation in smectic liquid-crystalline azobenzene molecules. *Nat. Commun.* **2019**, *10*, 1.

(88) Hada, M.; Shigeeda, Y.; Koshihara, S.-y.; Nishikawa, T.; Yamashita, Y.; Hayashi, Y. Bond Dissociation Triggering Molecular Disorder in Amorphous H2O. *J. Phys. Chem. A* **2018**, *122*, 9579.

(89) Hada, M.; Saito, S.; Tanaka, S. i.; Sato, R.; Yoshimura, M.; Mouri, K.; Matsuo, K.; Yamaguchi, S.; Hara, M.; Hayashi, Y.; et al. Structural monitoring of the onset of excited-state aromaticity in a liquid crystal phase. *J. Am. Chem. Soc.* **2017**, *139*, 15792.

(90) Sciaini, G.; Harb, M.; Kruglik, S. G.; Payer, T.; Hebeisen, C. T.; zu Heringdorf, F.-J. M.; Yamaguchi, M.; Horn-von Hoegen, M.; Ernstorfer, R.; Miller, R. D. Electronic acceleration of atomic motions and disordering in bismuth. *Nature* **2009**, *458*, 56.

(91) Vasileiadis, T.; Skountzos, E. N.; Foster, D.; Coleman, S. P.; Zahn, D.; Krečinić, F.; Mavrantzas, V. G.; Palmer, R. E.; Ernstorfer, R. Ultrafast rotational motions of supported nanoclusters probed by electron diffraction. *Nanoscale Horizons* **2019**, *4*, 1164.

(92) Ernstorfer, R.; Harb, M.; Hebeisen, C. T.; Sciaini, G.; Dartigalongue, T.; Miller, R. D. The formation of warm dense matter - experimental evidence for electronic bond hardening in gold. *Science* **2009**, *323*, 1033.

(93) Eichberger, M.; Schäfer, H.; Krumova, M.; Beyer, M.; Demsar, J.; Berger, H.; Moriena, G.; Sciaini, G.; Miller, R. D. Snapshots of cooperative atomic motions in the optical suppression of charge density waves. *Nature* **2010**, *468*, 799.

(94) Daoud, H.; Floettmann, K.; Miller, R. J. D. Compression of high-density 0.16 pC electron bunches through high field gradients for ultrafast single shot electron diffraction: The Compact RF Gun. *Struct. Dyn.* **2017**, *4*, No. 044016.

(95) Floettmann, K. Generation of sub-fs electron beams at few-MeV energies. *Nucl. Instrum. Methods Phys. Res., Sect. A* **2014**, *740*, 34.

(96) Manz, S.; Casandruc, A.; Zhang, D.; Zhong, Y.; Loch, R. A.; Marx, A.; Hasegawa, T.; Liu, L. C.; Bayesteh, S.; Delsim-Hashemi, H.; et al. Mapping atomic motions with ultrabright electrons: towards fundamental limits in space-time resolution. *Faraday Discuss.* **2015**, *177*, 467.

(97) Yang, J.; Yoshida, Y. Relativistic Ultrafast Electron Microscopy: Single-Shot Diffraction Imaging with Femtosecond Electron Pulses. *Adv. Condens. Matter Phys.* **2019**, *2019*, na.

(98) Weathersby, S.; Brown, G.; Centurion, M.; Chase, T.; Coffee, R.; Corbett, J.; Eichner, J.; Frisch, J.; Fry, A.; Gühr, M.; et al. Mega-electron-volt ultrafast electron diffraction at SLAC National Accelerator Laboratory. *Rev. Sci. Instrum.* **2015**, *86*, No. 073702.

(99) Maxson, J.; Cesar, D.; Calmasini, G.; Ody, A.; Musumeci, P.; Alesini, D. Direct measurement of sub-10 fs relativistic electron beams with ultralow emittance. *Phys. Rev. Lett.* **2017**, *118*, 154802.

(100) Daraszewicz, S. L.; Giret, Y.; Naruse, N.; Murooka, Y.; Yang, J.; Duffy, D. M.; Shluger, A. L.; Tanimura, K. Structural dynamics of laser-

irradiated gold nanofilms. *Phys. Rev. B: Condens. Matter Mater. Phys.* **2013**, *88*, 184101.

(101) Irie, M.; Fukaminato, T.; Matsuda, K.; Kobatake, S. Photochromism of diarylethene molecules and crystals: memories, switches, and actuators. *Chem. Rev.* **2014**, *114*, 12174.

(102) Galinis, G.; Strucka, J.; Barnard, J. C.; Braun, A.; Smith, R. A.; Marangos, J. P. Micrometer-thickness liquid sheet jets flowing in vacuum. *Rev. Sci. Instrum.* **2017**, *88*, No. 083117.

(103) Ekimova, M.; Quevedo, W.; Faubel, M.; Wernet, P.; Nibbering, E. T. A liquid flatjet system for solution phase soft-x-ray spectroscopy. *Struct. Dyn.* **2015**, *2*, No. 054301.

(104) Rogers, J.; Nelson, K. A new photoacoustic/photothermal device for real-time materials evaluation: An automated means for performing transient grating experiments. *Phys. B* **1996**, *219*, 562.

(105) Goodno, G. D.; Dadusc, G.; Miller, R. D. Ultrafast heterodyne-detected transient-grating spectroscopy using diffractive optics. *J. Opt. Soc. Am. B* **1998**, *15*, 1791.

(106) Baum, P.; Yang, D.-S.; Zewail, A. H. 4D visualization of transitional structures in phase transformations by electron diffraction. *Science* **2007**, *318*, 788.

(107) Carbone, F.; Baum, P.; Rudolf, P.; Zewail, A. H. Structural preablation dynamics of graphite observed by ultrafast electron crystallography. *Phys. Rev. Lett.* **2008**, *100*, No. 035501.

(108) Hafke, B.; Witte, T.; Brand, C.; Duden, T.; Horn-von Hoegen, M. Pulsed electron gun for electron diffraction at surfaces with femtosecond temporal resolution and high coherence length. *Rev. Sci. Instrum.* **2019**, *90*, No. 045119.

(109) Tinnemann, V.; Streubühr, C.; Hafke, B.; Kalus, A.; Hanisch-Blicharski, A.; Ligges, M.; Zhou, P.; von der Linde, D.; Bovensiepen, U.; Horn-von Hoegen, M. Ultrafast electron diffraction from a Bi (111) surface: Impulsive lattice excitation and Debye—Waller analysis at large momentum transfer. *Struct. Dyn.* **2019**, *6*, No. 035101.

(110) Gulde, M.; Schweda, S.; Storeck, G.; Maiti, M.; Yu, H. K.; Wodtke, A. M.; Schäfer, S.; Ropers, C. Ultrafast low-energy electron diffraction in transmission resolves polymer/graphene superstructure dynamics. *Science* **2014**, *345*, 200.

(111) Yang, J.; Zhu, X.; Wolf, T. J.; Li, Z.; Nunes, J. P. F.; Coffee, R.; Cryan, J. P.; Gühr, M.; Hegazy, K.; Heinz, T. F.; Centurion, M.; Wang, X. J.; Martinez, T.; et al. Imaging CF3I conical intersection and photodissociation dynamics with ultrafast electron diffraction. *Science* **2018**, *361*, 64.

(112) Wolf, T.; Sanchez, D.; Yang, J.; Parrish, R.; Nunes, J.; Centurion, M.; Coffee, R.; Cryan, J.; Gühr, M.; Hegazy, K.; Wang, X. J.; Martinez, T.; et al. The photochemical ring-opening of 1, 3-cyclohexadiene imaged by ultrafast electron diffraction. *Nat. Chem.* **2019**, *11*, 504.

(113) Ischenko, A. A.; Schafer, L.; Luo, J. Y.; Ewbank, J. D. Structural and vibrational kinetics by stroboscopic gas electron diffraction- The 193 nm photodissociation of CS2s. *J. Phys. Chem.* **1994**, *98*, 8673.

(114) Yang, J.; Beck, J.; Uiterwaal, C. J.; Centurion, M. Imaging of alignment and structural changes of carbon disulfide molecules using ultrafast electron diffraction. *Nat. Commun.* **2015**, *6*, 8172.

(115) Zandi, O.; Wilkin, K. J.; Xiong, Y.; Centurion, M. High current table-top setup for femtosecond gas electron diffraction. *Struct. Dyn.* **2017**, *4*, No. 044022.

(116) Siwick, B. J.; Dwyer, J. R.; Jordan, R. E.; Miller, R. J. D. An atomic-level view of melting using femtosecond electron diffraction. *Science* **2003**, *302*, 1382.

(117) Amini-Nik, S.; Kraemer, D.; Cowan, M. L.; Gunaratne, K.; Nadesan, P.; Alman, B. A.; Miller, R. J. D. Ultrafast Mid-IR Laser Scalpel - Protein Signals of the Fundamental Limits to Minimally Invasive Surgery. *PLoS One* **2010**, *5*, No. e13053.

(118) Petersen, H.; Gliese, A.; Stober, Y.; Maier, S.; Hansen, N.-O.; Kruber, S.; Eggert, D.; Tóth, M.; Gosau, T.; Schlüter, H.; Miller, R. J. D.; al, e.; et al. Picosecond Infrared Laser (PIRL) Application in Stapes Surgery—First Experience in Human Temporal Bones. *Otology Neurotology* **2018**, *39*, e224.

(119) Mo, M. Z.; Chen, Z.; Li, R.; Dunning, M.; Witte, B. B. L.; Baldwin, J. K.; Fletcher, L. B.; Kim, J. B.; Ng, A.; Redmer, R.; et al.

Heterogeneous to homogeneous melting transition visualized with ultrafast electron diffraction. *Science* **2018**, *360*, 1451.

(120) Liu, L. C.; Jiang, Y.; Mueller-Werkmeister, H. M.; Lu, C.; Moriena, G.; Ishikawa, M.; Nakano, Y.; Yamochi, H.; Miller, R. D. Ultrafast electron diffraction study of single-crystal (EDO-TTF) 2SbF6: Counterion effect and dimensionality reduction. *Chem. Phys. Lett.* **2017**, *683*, 160.

(121) Jiang, Y.; Liu, L. C.; Müller-Werkmeister, H. M.; Lu, C.; Zhang, D.; Field, R. L.; Sarracini, A.; Moriena, G.; Collet, E.; Miller, R. D. Structural dynamics upon photoexcitation in a spin crossover crystal probed with femtosecond electron diffraction. *Angew. Chem., Int. Ed.* **2017**, *56*, 7130.

(122) Zauleck, J. P.; de Vivie-Riedle, R. Constructing grids for molecular quantum dynamics using an autoencoder. *J. Chem. Theory Comput.* **2018**, *14*, 55.

(123) Woerner, M.; Zamponi, F.; Ansari, Z.; Dreyer, J.; Freyer, B.; Prémont-Schwarz, M.; Elsaesser, T. Concerted electron and proton transfer in ionic crystals mapped by femtosecond x-ray powder diffraction. *J. Chem. Phys.* **2010**, *133*, No. 064509.

(124) Schoenlein, R.; Elsaesser, T.; Holldack, K.; Huang, Z.; Kapteyn, H.; Murnane, M.; Woerner, M. Recent advances in ultrafast X-ray sources. *Philos. Trans. R. Soc., A* **2019**, *377*, 20180384.

(125) Barends, T. R.; Foucar, L.; Ardevol, A.; Nass, K.; Aquila, A.; Botha, S.; Doak, R. B.; Falahati, K.; Hartmann, E.; Hilpert, M.; et al. Direct observation of ultrafast collective motions in CO myoglobin upon ligand dissociation. *Science* **2015**, *350*, 445.

(126) Pande, K.; Hutchison, C. D.; Groenhof, G.; Aquila, A.; Robinson, J. S.; Tenboer, J.; Basu, S.; Boutet, S.; DePonte, D. P.; Liang, M.; et al. Femtosecond structural dynamics drives the trans/cis isomerization in photoactive yellow protein. *Science* **2016**, *352*, 725.

(127) Nango, E.; Royant, A.; Kubo, M.; Nakane, T.; Wickstrand, C.; Kimura, T.; Tanaka, T.; Tono, K.; Song, C.; Tanaka, R.; et al. A three-dimensional movie of structural changes in bacteriorhodopsin. *Science* **2016**, *354*, 1552.

(128) Nogly, P.; Weinert, T.; James, D.; Carbajo, S.; Ozerov, D.; Furrer, A.; Gashi, D.; Borin, V.; Skopintsev, P.; Jaeger, K.; et al. Retinal isomerization in bacteriorhodopsin captured by a femtosecond x-ray laser. *Science* **2018**, *361*, eaat0094.

(129) Kovacs, G. N.; Colletier, J.-P.; Grünbein, M.; Yang, Y.; Stensitzki, T.; Batyuk, A.; Carbajo, S.; Doak, R.; Ehrenberg, D.; Foucar, L.; et al. Three-dimensional view of ultrafast dynamics in photoexcited bacteriorhodopsin. *Nat. Commun.* **2019**, *10*, 3177.

(130) Coquelle, N.; Sliwa, M.; Woodhouse, J.; Schirò, G.; Adam, V.; Aquila, A.; Barends, T. R.; Boutet, S.; Byrdin, M.; Carbajo, S.; et al. Chromophore twisting in the excited state of a photoswitchable fluorescent protein captured by time-resolved serial femtosecond crystallography. *Nat. Chem.* **2018**, *10*, 31.

(131) Yu, X.; Yao, B.; Lei, M.; Gao, P.; Ma, B. Femtosecond laser-induced permanent anisotropy in bacteriorhodopsin films and applications in optical data storage. *J. Mod. Opt.* **2013**, *60*, 309.

(132) Fischer, T.; Hampp, N. A. Two-Photon Absorption of Bacteriorhodopsin: Formation of a Red-Shifted Thermally Stable Photoproduct F620. *Biophys. J.* **2005**, *89*, 1175.

(133) Minitti, M.; Budarz, J.; Kirrander, A.; Robinson, J.; Ratner, D.; Lane, T.; Zhu, D.; Glownia, J.; Kozina, M.; Lemke, H.; et al. Imaging molecular motion: Femtosecond x-ray scattering of an electrocyclic chemical reaction. *Phys. Rev. Lett.* **2015**, *114*, 255501.

(134) Ruddock, J. M.; Yong, H.; Stankus, B.; Du, W.; Goff, N.; Chang, Y.; Odate, A.; Carrascosa, A. M.; Bellshaw, D.; Zotev, N.; et al. A deep UV trigger for ground-state ring-opening dynamics of 1, 3-cyclo-hexadiene. *Science Adv.* **2019**, *5*, No. eaax6625.

(135) Stankus, B.; Yong, H.; Zotev, N.; Ruddock, J. M.; Bellshaw, D.; Lane, T. J.; Liang, M.; Boutet, S.; Carbajo, S.; Robinson, J. S.; et al. Ultrafast X-ray scattering reveals vibrational coherence following rydberg excitation. *Nat. Chem.* **2019**, *11*, 716.

(136) Yong, H.; Ruddock, J. M.; Stankus, B.; Ma, L.; Du, W.; Goff, N.; Chang, Y.; Zotev, N.; Bellshaw, D.; Boutet, S.; et al. Scattering off molecules far from equilibrium. *J. Chem. Phys.* **2019**, *151*, No. 084301.

(137) Ki, H.; Oang, K. Y.; Kim, J.; Ihee, H. Ultrafast x-ray crystallography and liquidography. *Annu. Rev. Phys. Chem.* **2017**, *68*, 473.

(138) Kim, K. H.; Kim, J. G.; Nozawa, S.; Sato, T.; Oang, K. Y.; Kim, T. W.; Ki, H.; Jo, J.; Park, S.; Song, C.; et al. Direct observation of bond formation in solution with femtosecond X-ray scattering. *Nature* **2015**, *518*, 385.

(139) Van Driel, T. B.; Kjær, K. S.; Hartsock, R. W.; Dohn, A. O.; Harlang, T.; Chollet, M.; Christensen, M.; Gawelda, W.; Henriksen, N. E.; Kim, J. G.; et al. Atomistic characterization of the active-site solvation dynamics of a model photocatalyst. *Nat. Commun.* **2016**, *7*, 13678.

(140) Haldrup, K.; Levi, G.; Biasin, E.; Vester, P.; Laursen, M. G.; Beyer, F.; Kjær, K. S.; Van Driel, T. B.; Harlang, T.; Dohn, A. O.; et al. Ultrafast X-ray scattering measurements of coherent structural dynamics on the ground-state potential energy surface of a diplatinum molecule. *Phys. Rev. Lett.* **2019**, *122*, No. 063001.

(141) Wolter, B.; Pullen, M. G.; Le, A.-T.; Baudisch, M.; Doblhoff-Dier, K.; Senftleben, A.; Hemmer, M.; Schröter, C. D.; Ullrich, J.; Pfeifer, T.; et al. Ultrafast electron diffraction imaging of bond breaking in di-ionized acetylene. *Science* **2016**, *354*, 308.

(142) Amini, K.; Sclafani, M.; Steinle, T.; Le, A.-T.; Sanchez, A.; Müller, C.; Steinmetzer, J.; Yue, L.; Saavedra, J. R. M.; Hemmer, M.; et al. Imaging the Renner−Teller effect using laser-induced electron diffraction. *Proc. Natl. Acad. Sci. U. S. A.* **2019**, *116*, 8173.

(143) Liu, X.; Amini, K.; Steinle, T.; Sanchez, A.; Shaikh, M.; Belsa, B.; Steinmetzer, J.; Le, A.-T.; Moshammer, R.; Pfeifer, T.; et al. Imaging an isolated water molecule using a single electron wave packet. *J. Chem. Phys.* **2019**, *151*, No. 024306.

(144) Feenberg, E., Harvard University, 1933.

(145) Weigert, S. How to determine a quantum state by measure-ments: the Pauli problem for a particle with arbitrary potential. *Phys. Rev. A: At., Mol., Opt. Phys.* **1996**, *53*, 2078.

(146) Ischenko, A. A.; Ewbank, J. D.; Schafer, L. Structural and vibrational kinetics by time-resolved gas electron diffraction: stochastic approach to data analysis. *J. Phys. Chem.* **1995**, *99*, 15790.

(147) Hillery, M.; O'Connell, R. F.; Scully, M. O.; Wigner, E. P. Distribution functions in physics: fundamentals. *Phys. Rep.* **1984**, *106*, 121.

(148) Leonhardt, U. *Measuring the Quantum State of Light*; Cambridge University Press, 1997.

(149) Natterer, F. *The Mathematics of Computerized Tomography*; SIAM, 2001.

(150) Ewbank, J. D.; Schäfer, L.; Ischenko, A. A. Structural and vibrational kinetics of photoexcitation processes using time resolved electron diffraction. *J. Mol. Struct.* **2000**, *524*, 1.

(151) Cahill, K. E.; Glauber, R. J. Density operators and quasiprobability distributions. *Phys. Rev.* **1969**, *177*, 1882.

(152) Richter, T. Direct sampling of a smoothed Wigner function from quadrature distributions. *J. Opt. B: Quantum Semiclassical Opt.* **1999**, *1*, 650.

(153) Ischenko, A. A.; Ewbank, J. D.; Schäfer, L. Structural kinetics by stroboscopic gas electron diffraction Part 1. Time-dependent molecular intensities of dissociative states. *J. Mol. Struct.* **1994**, *320*, 147.

(154) Yang, J.; Guehr, M.; Shen, X.; Li, R.; Vecchione, T.; Coffee, R.; Corbett, J.; Fry, A.; Hartmann, N.; Hast, C.; et al. Diffractive imaging of coherent nuclear motion in isolated molecules. *Phys. Rev. Lett.* **2016**, *117*, 153002.

(155) Hosler, E. R.; Leone, S. R. Characterization of vibrational wave packets by core-level high-harmonic transient absorption spectroscopy. *Phys. Rev. A: At., Mol., Opt. Phys.* **2013**, *88*, No. 023420.

(156) Wei, Z.; Li, J.; Wang, L.; See, S. T.; Jhon, M. H.; Zhang, Y.; Shi, F.; Yang, M.; Loh, Z.-H. Elucidating the origins of multimode vibrational coherences of polyatomic molecules induced by intense laser fields. *Nat. Commun.* **2017**, *8*, 735.

(157) Ischenko, A. A.; Tarasov, Y. I.; Schafer, L. Structural Dynamics of Free Molecules and Condensed Matter. Part I. Theory and Experimental Technique. *Fine Chem. Technol.* **2017**, *12*, 5.

(158) Ischenko, A. A.; Schaefer, L.; Ewbank, J. D. Tomography of the molecular quantum state by time-resolved electron diffraction. *Proc. SPIE* **1998**, *3516*, 580.

(159) Williamson, J. C.; Zewail, A. H. Ultrafast electron diffraction. 4. Molecular structures and coherent dynamics. *J. Phys. Chem.* **1994**, *98*, 2766.

(160) Leonhardt, U.; Raymer, M. Observation of moving wave packets reveals their quantum state. *Phys. Rev. Lett.* **1996**, *76*, 1985.

(161) Leonhardt, U.; Munroe, M.; Kiss, T.; Richter, T.; Raymer, M. Sampling of photon statistics and density matrix using homodyne detection. *Opt. Commun.* **1996**, *127*, 144.

(162) Hassan, M. T.; Baskin, J.; Liao, B.; Zewail, A. High-temporal-resolution electron microscopy for imaging ultrafast electron dynamics. *Nat. Photonics* **2017**, *11*, 425.

(163) Priebe, K. E.; Rathje, C.; Yalunin, S. V.; Hohage, T.; Feist, A.; Schäfer, S.; Ropers, C. Attosecond electron pulse trains and quantum state reconstruction in ultrafast transmission electron microscopy. *Nat. Photonics* **2017**, *11*, 793.

(164) Feist, A.; Echternkamp, K. E.; Schauss, J.; Yalunin, S. V.; Schäfer, S.; Ropers, C. Quantum coherent optical phase modulation in an ultrafast transmission electron microscope. *Nature* **2015**, *521*, 200.

(165) Hassan, M. T. Attomicroscopy: from femtosecond to attosecond electron microscopy. *J. Phys. B: At., Mol. Opt. Phys.* **2018**, *51*, No. 032005.

(166) Mouritzen, A. S.; Mølmer, K. Tomographic reconstruction of quantum states in N spatial dimensions. *Phys. Rev. A: At., Mol., Opt. Phys.* **2006**, *73*, No. 042105.

(167) Mouritzen, A. S.; Mølmer, K. Quantum state tomography of molecular rotation. *J. Chem. Phys.* **2006**, *124*, 244311.

(168) Marchesini, S. A unified evaluation of iterative projection algorithms for phase retrieval. *Rev. Sci. Instrum.* **2007**, *78*, No. 011301.

(169) Marchesini, S.; Tu, Y.-C.; Wu, H.-t. Alternating projection, ptychographic imaging and phase synchronization. *Appl. Comput. Harmonic Analys.* **2016**, *41*, 815.

(170) Pauli, W. *Handbuch der Physik*; Springer Verlag, 1933 (we keep Pauli's original notation x for the spatial coordinate).

(171) Pelz, P. M.; Qiu, W. X.; Bücker, R.; Kassier, G.; Miller, R. D. Low-dose cryo electron ptychography via non-convex Bayesian optimization. *Sci. Rep.* **2017**, *7*, 9883.

(172) Kowalewski, M.; Bennett, K.; Dorfman, K. E.; Mukamel, S. Catching conical intersections in the act: Monitoring transient electronic coherences by attosecond stimulated X-ray Raman signals. *Phys. Rev. Lett.* **2015**, *115*, 193003.

(173) Kowalewski, M.; Bennett, K.; Mukamel, S. Monitoring nonadiabatic avoided crossing dynamics in molecules by ultrafast X-ray diffraction. *Struct. Dyn.* **2017**, *4*, No. 054101.

(174) Dixit, G.; Vendrell, O.; Santra, R. Imaging electronic quantum motion with light. *Proc. Natl. Acad. Sci. U. S. A.* **2012**, *109*, 11636.

(175) Henriksen, N. E.; Møller, K. B. On the theory of time-resolved x-ray diffraction. *J. Phys. Chem. B* **2008**, *112*, 558.

■ NOTE ADDED AFTER ASAP PUBLICATION

This paper was published ASAP on January 9, 2020, and it was missing some of the authors' corrections. The corrected version was reposted on January 17, 2020.